Summer 2011

Improving the Efficiency of Organic Solar Cells by Varying the Material Concentration in the Photoactive Layer

Kevin Anthony Latimer
Old Dominion University

IMPROVING THE EFFICIENCY OF ORGANIC SOLAR CELLS BY VARYING THE MATERIAL CONCENTRATION IN THE PHOTOACTIVE LAYER

by

Kevin Anthony Latimer
B.S. August 2010, Old Dominion University

A Thesis Submitted to the Faculty of
Old Dominion University in Partial Fulfillment of the
Requirements for the Degree of

MASTER OF SCIENCE

ELECTRICAL AND COMPUTER ENGINEERING

OLD DOMINION UNIVERSITY
August 2011

Approved by:

Gón Namkoong (Director)

Helmut Baumgart (Member)

Sylvain Marsillac (Member)

ABSTRACT

IMPROVING THE EFFICIENCY OF ORGANIC SOLAR CELLS BY VARYING THE MATERIAL CONCENTRATION IN THE PHOTOACTIVE LAYER

Kevin Anthony Latimer
Old Dominion University, 2011
Director: Dr. Gon Namkoong

Polymer-fullerene bulk heterojunction solar cells have been a rapidly improving technology over the past decade. To further improve the relatively low energy conversion efficiencies of these solar cells, several modifications need to be made to the overall device structure. Emerging technologies include cells that are fabricated with interfacial layers to facilitate charge transport, and tandem structures are being introduced to harness the absorption spectrum of polymers with varying bandgap energies.

When new structures are implemented, each layer of the cell must be optimized in order for the entire device to function efficiently. The most volatile layer of these devices is the photoactive layer solution of poly-3(hexylthiophene-2,5-diyl) (P3HT) and [6,6]-phenyl-C_{61}-butyric acid methyl ester ($PC_{61}BM$). Even slight variations in pre-application and post-treatment will lead to large variations in the electrical, physical, and optical properties of the solar cell module.

To improve the effectiveness of the photoactive layer, the material concentration of P3HT and $PC_{61}BM$ in the liquid phase, prior to application, was altered. The weight ratio of P3HT to $PC_{61}BM$ was kept at a constant 1 to 0.8, while the amounts of each dissolved in 2 mL of chlorobenzene were varied. Solar cells were fabricated, and J-V characterizations were performed to determine the electrical traits of the devices. Atomic force microscopy (AFM) measurements were done on the photoactive layer films to

determine the physical characteristics of the films such as overall surface topology and RMS roughness. Also, variable angle spectroscopic ellipsometry (VASE) was used to determine film thickness and extinction coefficient of the active layers. To further understand the optical properties of the polymer-fullerene blend, the absorption spectrum of the films were calculated through UV-VIS spectrophotometry.

It was found that an increased concentration of the polymer-fullerene blend prior to application increased overall device efficiency. A photoactive layer solution prepared with 30 mg P3HT and 24 mg $PC_{61}BM$, when implemented in an organic solar cell, produced the optimal electrical, physical, and optical characteristics.

ACKNOWLEDGEMENTS

There are several people to whom I wish to extend thanks for helping me throughout the completion of this thesis. First and foremost, I thank Dr. Gon Namkoong for allowing me to conduct research in his laboratory and for originally sparking my interest in the field of semiconductors and solid state electronics. I am grateful to have done such interesting, meaningful research under a director with a genuine interest in his work. I would also like to thank my committee members, Dr. Helmut Baumgart and Dr. Sylvain Marsillac, for their input and guidance during completion of this thesis. I also wish to extend thanks to Dr. Tarek Abdel-Fattah for our discussions and collaboration during the data collection process.

I owe several thanks to the gentleman that I have worked with at the ARC while completing this thesis. Utmost thanks go to Pat Boland and Kurnia Fu for being excellent teachers and co-workers over the past year. Special thanks also go to Dr. Diefeng Gu and Dr. Wei Cao for their teaching and help. I would also like to extend my gratitude to Vikash, Thomas, Alex, and Jessica for helping me with various aspects of the data collection.

I am further indebted to my parents, Keith and Heidi Latimer, for putting my education first and foremost in their lives, teaching me at a young age the importance of math and science, and always being positive and encouraging towards all of my decisions in life. I would also like to thank my girlfriend of over 6 years, Lauren, for always being supportive of my academic endeavors.

NOMENCLATURE

2-D	2-Dimensional
3-D	3-Dimensional
AFM	Atomic Force Microscopy
BHJ	Bulk Heterojunction
FF	Fill Factor (%)
HOMO	Highest Occupied Molecular Orbital
ITO	Indium Tin Oxide
J	Current Density (mA/cm^2)
J_{MAX}	Current Density at the Maximum Power Point
J_{SC}	Short Circuit Current Density (mA/cm^2)
k	Extinction Coefficient (unitless)
LUMO	Lowest Unoccupied Molecular Orbital
MPP	Maximum Power Point (mW)
$\tilde{N}$	Complex Index of Refraction
n	Refractive Index (unitless)
OSC(s)	Organic Solar Cell(s)
P3HT	Poly(3-hexylthiophene-2,5-diyl)
$PC_{61}BM$	[6,6] Phenyl C_{61} Butyric Acid Methyl Ester
PCBM	[6,6] Phenyl C_{61} Butyric Acid Methyl Ester
PEDOT:PSS	Poly(3,4-ethylenedioxythiophene):poly(4-styrenesulfonate)
PCE	Percent Efficiency (%)
PV	Photovoltaic
RMS	Root Mean Square
RPM	Revolutions per Minute (rev/min)
R_S	Series Resistance (Ω)
R_{SH}	Shunt Resistance (Ω)
SE	Spectroscopic Ellipsometry
TEM	Tunneling Electron Microscope
UV	Ultraviolet
UV-Vis	Ultraviolet-Visible
VASE	Variable Angle Spectroscopic Ellipsometry
V_{MAX}	Voltage at the Maximum Power Point (V)
V_{OC}	Open-Circuit Voltage (V)
XRD	X-Ray Diffraction

TABLE OF CONTENTS

LIST OF TABLES

LIST OF FIGURES

CHAPTER I

INTRODUCTION

I.1 Solar Cell History

The history of solar cells dates back to as early as 1839, when scientist Edmond Bequerel observed current flow through two illuminated electrodes that were submerged in water [1]. Since then, a great deal of research and development on photovoltaic (PV) modules has been done, with the most significant progress coming from large research groups such as Bell Laboratories [2] and government research teams [3]. In the 1800s and well into the 1900s, there was minimal understanding of the solid state physics behind solar cell operation. The technology was raw and undeveloped but a popular research interest; the ability to harness the limitless, clean power of the sun was a very attractive option for a growing energy market [4].

Some of the main factors that pushed for the development of solar energy in recent decades have been the applications of solar panels in the aeronautics industry [5] and the oil crisis in the 1970s [1]. The volatile nature of the petroleum market has produced an interest in developing a more sustainable, renewable form of energy [6,7]. On top of this, the increasing concerns of global warming have demanded the development of a cleaner source of energy [8].

Today, the market for solar cells is dominated by silicon-based modules. Monocrystalline silicon panels have efficiencies of almost 25% [9,10], lifetimes of up to 30 years [10], and virtually no maintenance or upgrade costs, making them an attractive renewable energy option [11]. However, silicon panels do have their caveats.

Approximately 70% of the cost of a silicon solar panel lies in the wafer production [12]. Also, the shortages of silicon feedstock have pushed the industry to spend money developing new ways to produce solar-grade silicon [12].

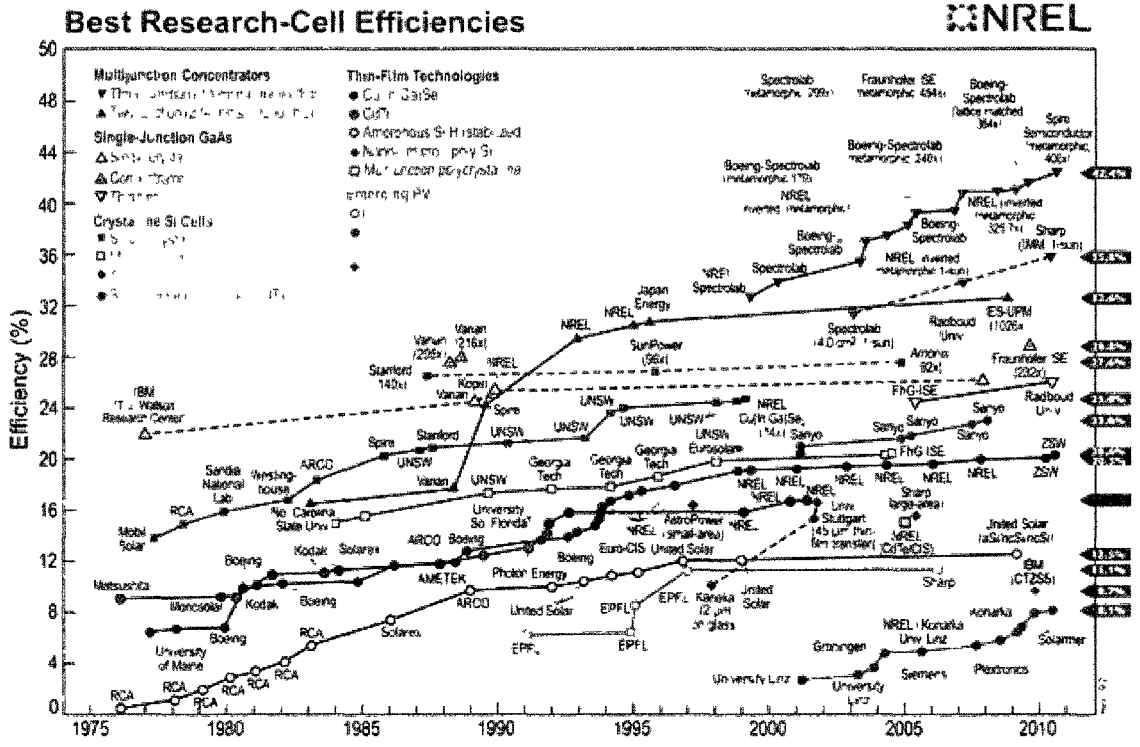

Figure I.1: Record PV cell efficiencies since 1975 [9]

Furthermore, the efficiencies of silicon solar cells have remained stagnant. As shown in Figure I.1, the efficiencies of single crystal silicon solar cells have been stuck in the 20-25% range since the 1980s [9]. Similar to the global energy market, it would be wise to develop new PV technologies to supplement the field. Diversification of the solar cell market will allow emerging technologies to fill the niches that silicon based modules cannot [13], making the field of solar energy more robust. In response to this, other types of non-silicon research cells have been developed over the past few decades

including a variety of solid inorganic thin film technologies [14,15], dye-sensitized cells [16], and organic solar cells [17].

I.2 Organic Solar Cells

Organic Solar Cells (OSCs) are an emerging PV technology that could soon challenge the dominance of silicon based modules [4,6,18,19]. OSCs are thin film devices that are comprised of carbon-based chemicals. While the two electrodes of the cells are solid films of metal or metal oxide, the organics that make up the bulk of the cell can be processed in solution form [4]. The layer that harvests electrons is the photoactive layer, and is a combination of two organic chemicals: the polymer poly(3-hexylthiophene-2,5-diyl) (P3HT) and the fullerene derivative [6,6] phenyl C_{61} butyric acid methyl ester ($PC_{61}BM$) [20]. These two chemicals are dissolved in an organic solvent and spin coated onto the substrate of the cell. The purpose of these two chemicals is to absorb light from the sun, generate free electron-hole pairs, and transport them to the charge collection interfaces [20].

The organic solar cell offers unique advantages over their silicon counterparts. Since the bulk of the solar cell is applied in solution form, production can be speedy and low in cost [4,13]. Also, the substrates that the cells are fabricated on can be flexible plastic, opening up endless possibilities of large-area solar panels [13,21]. The OSC structures are also thin and lightweight; in the future, it is possible that organic PV (OPV) modules could be mounted on buildings, satellites, cars, and other inanimate objects without adding increased bulk.

Referring back to Figure I.1, the efficiency of OPV modules has increased from 2.5% [21] to 7.4% [22] over the past decade. Due to the flexible nature of the device structures and polymer chemistry [18], novel improvements have propelled the research forward. In 1995, it was discovered that mixing the polymer and fullerene together in the same blend produced an efficient electron donor-acceptor network [23], referred to as a bulk heterojunction (BHJ). As seen in Figure I.1, exponential increases in efficiencies, which correspond to further innovations in organic solar cell physics, began in 2003 and 2009. In 2003, scientists began to use a new polymer in the active layer [20], and in 2009, researchers began stacking cells on top of one another to form tandem structures [24]. This type of innovation shows that slight alterations in the physical structure and composition of polymer solar cells lead to novel and improved devices over time.

I.3 Challenges Facing Organic Solar Cell Technology

Unfortunately, there are several more obstacles to overcome before OPV modules can be a marketable product. The two main problems with the technology right now are low device efficiencies and severe degradation of the modules in ambient air. Even after a few hours in the atmosphere [25,26], the solar cell efficiency begins to suffer, stemming from the accumulation of water in the organic polymers [25] and the breakdown of the polymer-cathode interface [26].

The low efficiency of these polymer solar cells comes from the limitations of the photoactive layer materials. The bandgap energy of a material is the required energy to excite an electron from the highest occupied molecular orbital (HOMO) to the lowest

unoccupied molecular orbital (LUMO), which can ultimately result in current flow [19]. For most organic semiconductors, the bandgap energy is greater than or equal to 2 eV, which is high for PV applications; because of this, the wavelengths that the active layer can absorb are severely limited [27]. This spectral mismatch leads to low charge carrier concentration and, in turn, low current density and low efficiency [17]. In efforts to remedy this, scientists in 2003 implemented the new polymer P3HT into the photoactive layer [28], which has band gap energy just under 2 eV. This extended the absorption spectrum of the photoactive layer to higher wavelengths in the visible spectrum and into the near infrared range (700 nm).

Another limitation in OSC efficiency is the carrier lifetime of electron-hole pairs (excitons) generated in the active layer. Once the excitons are generated, they must quickly diffuse to the interfaces before they lose energy and recombine [4]. For typical semiconducting polymers, the diffusion length for photo-generated excitons is around 10 nm, with lifetimes in the nanosecond range [4,29].

I.4 Goal and Outline of Thesis Research

As stated earlier, the major limitations of the device efficiency of polymer solar cells are the limited absorption profile of the organics in the active layer [27] and the short carrier lifetime of the charges [4,29]. In this thesis research, it is proposed that by increasing the concentration of chemicals (P3HT and PCBM) in the photoactive layer blend, the device efficiency will increase due to a higher degree of absorption.

If an increased amount of polymer and fullerene are in the active layer, the incoming photons will have more molecules to excite, which will generate more

excitons [30]. Since the network of polymer and fullerene will be more densely packed, the charges will also have greater mobility due to the increased crystalline nature of the active layer. One limitation of this experiment will be how dense the layer can be packed; increased active layer density will result in a thicker photoactive layer. If the layer is too thin, absorption will be limited, but a larger percentage of the excitons will be able to diffuse to the interfaces. Conversely, if the active layer is too thick, the excitons will suffer from recombination and stray resistances [4,31] before they can diffuse to the charge collecting interfaces. Studies report [4,32] that the optimal thickness of the photoactive layer in this structure of polymer solar cells lies in the range of 60-100 nm.

In this thesis, the effects of increasing the active layer density on solar cell performance will be investigated. Four different photoactive layer blends with varying concentrations will be tested. For each active polymer, solar cells will be fabricated and characterized electrically to calculate the percent efficiency (PCE). Several cells will be fabricated for each polymer blend to determine the optimal thickness for each unique blend. Once the optimal film thicknesses for the four photoactive layer blends have been determined, additional characterization techniques will be employed to learn more about the underlying physical and optical characteristics.

Atomic force microscopy (AFM) will be used to view physical topology and roughness of the active layers. Spectroscopic ellipsometry (SE) and ultra-violet-visible (UV-Vis) spectrophotometry measurements will be used to determine overall absorption spectrum, extinction coefficient values, and where the local absorption peaks are for each active layer blend. Understanding the underlying physical and optical properties of

the photoactive layers will provide a thorough explanation as to why certain active layers are more efficient than others.

CHAPTER II

SOLAR CELL PHYSICS

II.1 Introduction

To fully understand the study at hand, a fundamental knowledge of organic solar cell physics is crucial. This section will briefly describe the charge transport mechanisms in conjugated chemical systems. An in-depth description of the photoactive layer contents (P3HT and PCBM) will be provided. Furthermore, a description of the overall device structure will be given, and operation of the OSC will be explained.

II.2 Conjugated Chemical Systems

The unique electrical properties exhibited by organic semiconductors stem from the alternating single and double bonds among the carbon atoms in the materials [4,33], which by definition is a conjugated system. The two most frequently occurring covalent bonds between molecules are sigma (σ) and pi (π) bonds. Sigma bonds are characterized by the electron orbitals of the two atoms being lined up along the same axis, and pi bonds occur when remaining p-orbitals overlap on one of the axes.

For typical conjugated organic semiconductors, including the ones used in polymer solar cells, a single carbon atom will have either two or three neighboring atoms and always two neighboring carbons [33,34,35]. The formation of the pi bonds is due to the alternating single and double bond nature of conjugated polymers and the valence structure of carbon ($2s^2\ 2p^2$). When two carbons have a single bond, this means that they will be double bonded with the carbons on the opposite sides. Therefore, each

carbon will be sharing a total of 3 electrons and will be sigma bonded on 3 different axes. The 2 s-orbital electrons will bond first, and one of the p-orbital electrons will bond, leaving one remaining p-orbital electron in the valence band of both carbons. The overlapping of these remaining p-orbital electrons is by definition a pi bond [4,36].

The alternating pi bonds among the carbons throughout the polymer are said to be delocalized in nature, which means that they do not belong to a specific atom [4,37]. The flexibility of the delocalized pi electrons is of special interest to polymer physics and especially in solar cell applications because pi-bonded electrons can readily absorb photons and create photogenerated charge carriers [4,35]. Furthermore, when a delocalized pi system is brought into contact with another donor or acceptor material, it has been observed that the conductivity of the conjugated polymer increases, changing the electric properties of the chemical from an insulator to that of a conductor [37]. Also, since the pi bonds are significantly weaker than the sigma bonds, the bandgap energy of the polymer is characterized by the energy required to excite a pi bonded electron from the HOMO to the LUMO [4]. The sigma bonds, which are still rather important, provide electrochemical stability for the polymer [4].

Both P3HT and PCBM are materials that have a conjugated base structure. Also, the hole transporting layer in the cell, poly(3,4-ethylenedioxythiophene):poly(4-styrenesulfonate) (PEDOT:PSS), is comprised of thiophene and styrene chains, which are also conjugated polymers. The delocalized pi electrons in these polymers give them their unique semiconducting properties and make them suitable choices for OSC applications [4,33,35,37].

II.3 Photoactive Layer Composition

Traditional solid state donor-acceptor systems occur at an abrupt p-n junction [33,38]. When electron-hole pairs are generated, it is the job of the p-type material to transport the holes, and the n-type material to transport electrons. The bulk heterojunction structure, on the other hand, provides an intertwined network of donor and acceptor molecules [23,27], which are P3HT and PCBM in modern organic solar cells.

II.3.1 P3HT

Poly(3-hexylthiophene-2,5-diyl) (P3HT) is a conjugated polymer that is used as a hole transporter in the photoactive layer blend [39]. Alone, a thiophene chain is not soluble in common organic solvents, nor is any conjugated polymer [23]. Since the photoactive layer is to be solution processable, a side chain (C_6H_{13}) is added onto the third carbon atom (counting clockwise from the sulfur atom), making the molecule soluble in common organic solvents such as 1- or 2-chlorobenzene or chloroform [34].

The 2,5-diyl suffix on the name of the polymer corresponds to the second and fifth molecules (still counting clockwise starting with the sulfur) joining the thiophenes together; this 2,5 structure is known as a head-to-tail configuration [34]. Other configurations such as head-to-head and tail-to-tail can alter the alignment of the thiophene bonds, resulting in lower levels of conjugation, and increased energy bandgaps [23,34].

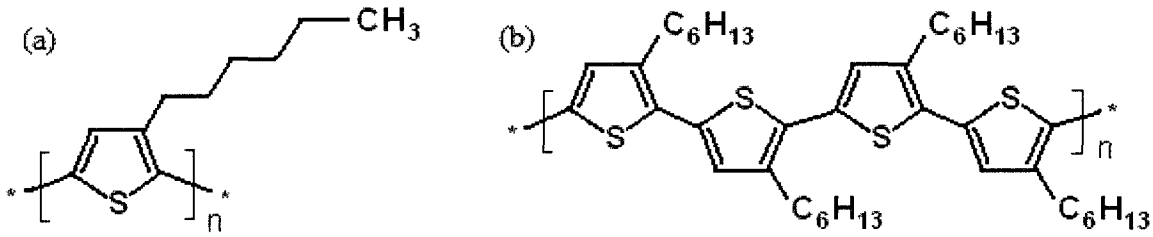

Figure II.1: (a) A monomer of the P3HT polymer, and (b) regioregular P3HT structure

A thiophene chain exhibits the highest levels of optical absorption when the thiophenes are joined together in successive head to tail fashion [24]. The percentage of monomers in the polymer that are joined in a head to tail fashion is referred to as the degree of regioregularity in the polymer [40,41]. Figure II.1 pictorially shows a single monomer of P3HT and also the regioregular structure of the polymer. Due to imperfections in the synthesis process, 100% regioregularity is not possible, but electronic grade P3HT will have regioregularity values in the 90-94% range, according to Rieke Metals, Inc., the manufacturer from which P3HT is obtained. Increased regioregularity in the P3HT leads to favorable electrochemical properties such as increased lamellar stacking, a higher degree of conjugation, and a higher absorption coefficient, all leading to more efficient hole transport in OSC applications [23,24,40,42].

II.3.2 $PC_{61}BM$

[6,6] Phenyl C_{61} butyric acid methyl ester ($PC_{61}BM$, or PCBM) is a fullerene derivative used as an electron acceptor in OSC applications [27]. The 60 carbons that make up the body of the derivative are the perfectly spherical buckminsterfullerene C_{60}, which is a very stable structure [43,44,45]. The highly conjugated system is very stable because of the nearly identical bond lengths among the carbons due to the spherical

nature of the molecule, resulting in few or no delocalized electrons [44,45]. A single molecule of PCBM is shown in Figure II.2 to demonstrate its spherical symmetry and highly conjugated nature.

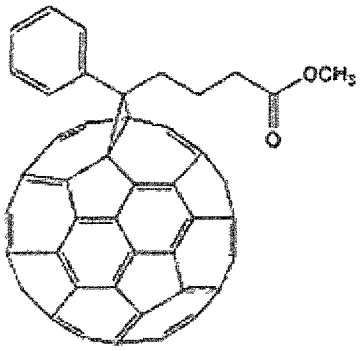

Figure II.2: The fullerene derivative $PC_{61}BM$

To make the fullerene soluble, and to also fine-tune the electrical properties of the chemical, a side chain is added onto the body [44]. The [6,6] notation means that during processing of PCBM, the side chain is added in a "closed loop" fashion, making the molecule a methanofullerene [44]. Although adding the side chain slightly decreases stability by breaking the conjugation of the carbons, it is the only option that produces a stable, soluble fullerene [44]. The spherical shape of the fullerene derivative is advantageous because in charge transport systems, molecules have good contacts with their surroundings no matter what the orientation of the molecule is [45].

II.4 Organic Solar Cell Structure

As discussed, the photoactive layer of the OSC consists of the bulk heterojunction structure of P3HT and PCBM. Other materials must also be employed to

transport the holes and electrons to the electrodes. The substrate on which the cells will be fabricated is glass, which provides a transparent base that allows photons to pass through with minimal diffraction. On top of the glass is the transparent conducting oxide indium tin oxide (ITO), which is the anode of the structures [46]. According to the manufacturer of the ITO-patterned glass, NanoCS, the 100 nm films of ITO exhibit optical transmittance of over 80%, which allows for superior photon transmission to the active layer. On top of this, ITO exhibits high conductivity [47] and has a work function of 4.7 eV [46], which makes it an ideal choice for an anode in OSC structures.

On top of the ITO layer is a thin film of poly(3,4-ethylenedioxythiophene): poly(4-styrenesulfonate) (PEDOT:PSS) [47]. The PEDOT:PSS is actually a donor-acceptor network in itself [48]; the PEDOT, similar to P3HT, has a thiophene backbone and transports holes to the anode. The PEDOT is blended with the electron-accepting PSS to form a soluble chemical that can be spin coated onto a substrate [48]. This means that PEDOT:PSS is not only a hole transporting layer but also an electron blocker. The HOMO of PEDOT:PSS has an energy of 5.2 eV [46].

On top of the PEDOT:PSS layer is the photoactive layer, which is the interpenetrating network of P3HT and PCBM. P3HT has a HOMO of 4.9 eV and a LUMO of 3.0 eV, and PCBM has a HOMO and LUMO of 6.1 and 3.7 eV, respectively [46]. Since the LUMO of the PCBM is lower than that of P3HT, the PCBM acts as the electron transporter, and the P3HT acts as the hole transporter [45]. Lastly, the structure is capped off with aluminum, which has a work function of 4.2 eV [46].

The work function of aluminum is slightly higher than the LUMO of the PCBM (3.7 eV), which will facilitate smooth electron transport from the fullerene to the

aluminum cathode. The HOMO energy of P3HT (4.9 eV) is in the range of the HOMO of PEDOT:PSS (5.2 eV) and the work function of ITO (4.7 eV). The energy bands lining up in this fashion allow for increased hole transport through the layers to the anode. Figure II.3 graphically shows the physical structure of the layers of the OSC and the pertinent energy levels of the materials.

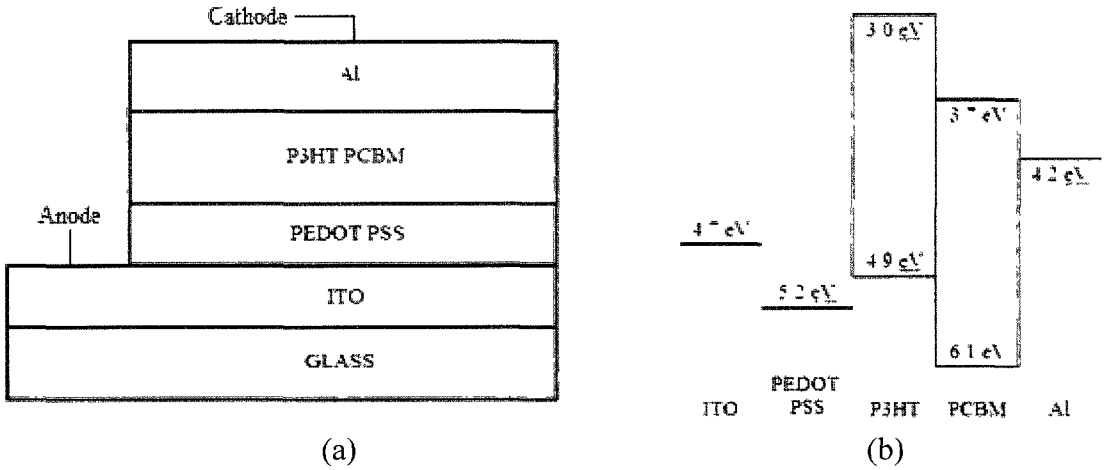

Figure II.3: (a) The physical structure and (b) the energy band structure of an OSC

II.5 Operation of an Organic Solar Cell

The operation of an OSC begins with incoming photons striking the active layer. The light travels through the glass, ITO, and PEDOT:PSS layers, and stimulates the pi-bonded electrons in the photoactive layer. If the light is neither absorbed by the active layer contents nor diffracted out of the cell, the photons will reflect off of the aluminum and travel back through the active layer, enabling the photons another chance to be absorbed [4]. Due to relatively high band gap energies of organic semiconductors, only about 30% of the incident solar irradiation is harvested; to make up for this, organics tend to have much higher absorption coefficients [4]. If the wavelengths from the

source of illumination are absorbed by the P3HT:PCBM network and contain energy greater than or equal to the band gap energy of the P3HT or PCBM, an exciton will form [49].

Next, the electron-hole pair will diffuse to the charge collecting interfaces [4]. Due to the nature of the bulk heterojunction structure, the interface is not a single entity but a conglomeration of polymer-fullerene interfaces throughout the photoactive layer. As detailed earlier, the diffusion length of photogenerated excitons in conducting polymers is around 10 nanometers, and the lifetime is typically in the order of nanoseconds [4,29]. If the exciton fails to diffuse to an interface, the electron-hole pair will recombine [48].

Assuming that the exciton diffuses to a P3HT-PCBM interface, the electron-hole pair will dissociate into separate charges due to the desire of excitons to reach a lower-energy state [36]. If an electron travels from the LUMO of the donor to the LUMO of the acceptor, or if a hole moves from the HOMO of the acceptor to the HOMO of the donor, then the exciton will have effectively reduced its overall energy by dissociating the electron-hole pair [36]. Now that the charges are separated, they must traverse the layers to the electrodes. The free charges are transported towards the anode and cathode due to the induced electric field in the device, caused by the energy band bending of the semiconductor materials [36].

The detailed physics of an organic solar cell are illustrated in Figure II.4. Because the area between donor and acceptor molecules in a polymer-fullerene solar cell is on the order of 10 nm [50], the bulk of the OSC device operates in the depletion region. There is a built in voltage in the structure due to the induced electric field in the

device, which is caused by the varying work functions of the electrodes. ITO is a high work function (4.7 eV) electrode, and aluminum is a low work function (4.2 eV) electrode. The LUMO and HOMO of the bulk of the cell bend so that the HOMO of the heterojunction is lined up with the ITO anode, and the LUMO of the bulk lines up with the aluminum cathode. Figure II.4 is displayed below to graphically show how the entire bulk of the material bends the HOMO and LUMO bands and to show how the induced electric field transports the charges to the electrodes.

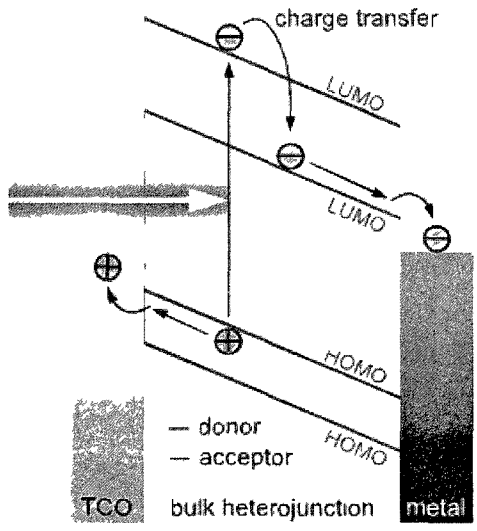

Figure II.4: Band bending in a bulk heterojunction solar cell; upon exciton dissociation, the bending of the LUMO and HOMO transport the charges to the electrodes

The holes will traverse the P3HT polymer and travel through the PEDOT:PSS layer and ITO to be collected at the anode, and the electrons will be transported from the PCBM to the aluminum cathode. The continuous collection of holes by the ITO and electrons by the aluminum results in current flowing through the device. This

complicated process of electron-hole behavior in an OSC is detailed in Figure II.5.

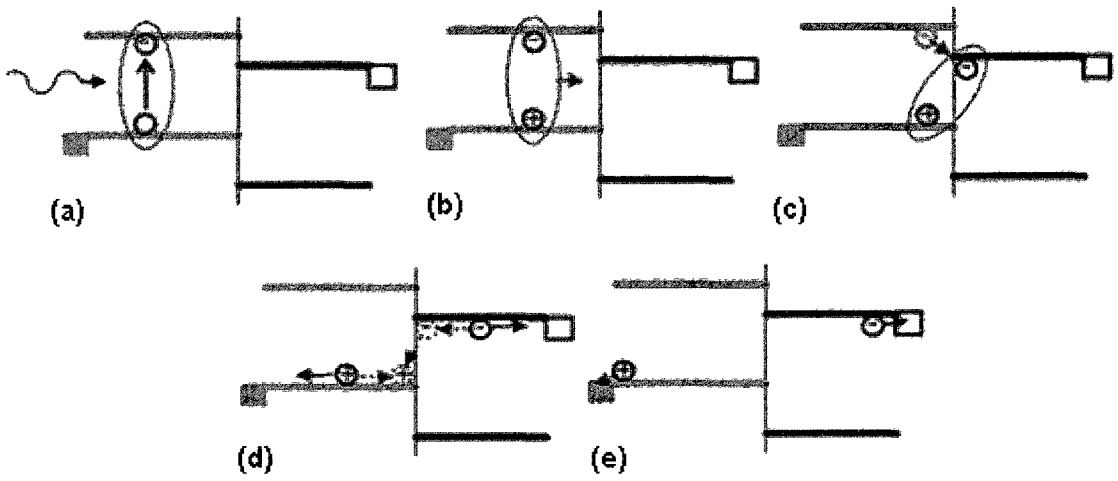

Figure II.5: (a) Photon absorption and exciton formation, (b) diffusion to the donor-acceptor interface, (c) charge dissociation, (d) charge transport, and (f) collection

The charge transport through the layers is impeded by various recombination schemes, including imperfections in the bulk heterojunction structure, and limitations in the active layer contents. As stated earlier, the bulk heterojunction structure provides a crystalline, interpenetrating network of polymer and fullerene. Although theoretically sound, it is very difficult to actually control the physical morphology of the polymer and fullerene once they are cast onto a solar cell. It is known that thermal annealing of the active layer will produce a more crystalline network [27,30,51], but studies also show that the fullerene tends to migrate to the bottom of the active layer and the polymer to the top [52]. This is problematic because if the bulk of the PCBM is located at the bottom of the photoactive layer, there will be insufficient fullerene to transport the electrons to the cathode; similarly, if disproportional amounts of polymer are at the top of the heterojunction, it will be more difficult for the holes to migrate towards the anode.

Another limitation in the charge transport of bulk heterojunction polymer solar cells is the varying charge mobilities of the heterojunction materials. Hole mobility for P3HT is in the range of 2×10^{-8} $m^2V^{-1}s^{-1}$, and the electron mobility of PCBM is around 3×10^{-7} $m^2V^{-1}s^{-1}$ [39]. The Langevin expression is typically used to determine the biomolecular recombination rate of free charge carriers in organic semiconductors and depends mainly on the mobilities of the holes and electrons [53]. Recent studies have concluded that this recombination rate does not depend on both the hole and electron mobility but whichever charge has the lowest mobility [53]. For steady current flow, the nummber of holes collected at the anode must equal the electrons at the cathode. If the holes can only be transported to the PEDOT:PSS layer at a rate of 2×10^{-8} $m^2V^{-1}s^{-1}$, then the electrons will be collected by the aluminum at the same rate; the remaining electrons will be forced to recombine [53].

Charge transport in bulk heterojunction solar cells is obviously a volatile process and is directly affected by the composition of the active layer. Throughout the literature, various parameters such as weight ratio [20,29,54], choice of solvent [55], and film thickness [32] of the photoactive layer have been investigated and optimized to maximize the current density and, subsequently, the PCE of the OSCs. It has been determined that the weight ratio of P3HT:PCBM should be in the range of 1:0.8 to 1:1 [20,29,54], chlorobenzene should be used as the solvent [55], and the film thickness should lie in the range of 60-100 nm [4,32]. While these current-limiting effects have been thoroughly investigated, one variable that has not been extensively studied is the concentration of the active layer solution prior to deposition. This thesis study proposes that by increasing the concentration of the polymer and fullerene in the photoactive layer

solution prior to deposition, these effects that limit the photocurrent density could possibly be combated. By increasing the concentration of the materials in the thin film, the crystalline nature of the polymer-fullerene network and contact area among the charge carries could improve. This will in turn increase the absorption of photons in the photoactive layer, the current density of the solar cells, and also the overall device efficiency.

CHAPTER III

EXPERIMENTAL SETUP

III.1 Introduction

The pertinent physics background of organic solar cell technology has been discussed. Several characterization methods will be employed to determine the various electrical, physical, and optical characteristics of organic solar cells, and the photoactive layer thin films of those solar cells. This section will first detail the fabrication procedures for an organic solar cell. Secondly, each characterization method will be explored, and its significance in determining properties of the OSC or the photoactive layer thin film will be explained.

III.2 Fabrication of Organic Solar Cells

Glass slides are purchased from NanoCS that have been patterned with 100 nanometers of ITO (10 ohm/sq). The slides are broken into 1 inch squares in preparation for chemical etching. To protect the ITO substrate, silicone tape (0.25 inch width) is placed in two parallel strips on the slide. The ITO slide is submerged in a heated (50° C) solution of 25% HCl and 75% deionized water to remove the exposed oxide.

Before materials can be deposited on the substrate, a thorough cleaning of the slide must be done to remove any native surface impurities. Ultrasonic treatments of the slide are performed in a 3% Mucasol solution, deionized water, acetone, and ethanol, and the slide is then baked to remove any residual moisture.

The PEDOT:PSS (electronic grade Clevios P VP Al 4083 purchased from Heraeus) is then cast onto the substrate by a vacuum-type spin coating machine. The PEDOT:PSS is spun onto the cleaned, etched ITO substrate for 3 minutes at a terminal velocity of 3000 rpm and a ramp speed of 500 rpm/s. After application, a thin strip of PEDOT:PSS is removed with acetone to expose the anode, and the backside of the slide is cleaned as well. To get rid of the film of water, and to increase the conductivity of the PEDOT:PSS [56], the cell is baked in a nitrogen glovebox (<1 ppm O_2 and H_2O) for ten minutes at 100° C.

Prior to processing, the photoactive layer solution must be prepared. The variables of interest in this thesis research are the amounts of polymer and fullerene that are dissolved in the active layer solution prior to deposition. Table III.1 outlines the four photoactive layer solutions that will be tested throughout this research.

Table III.1: The contents of the four photoactive layer solutions

Active Layer Solution	P3HT (mg/2mL)	PCBM (mg/2mL)
1	20	16
2	25	20
3	30	24
4	35	28

Keeping the weight ratio of P3HT to PCBM at a constant 1:0.8, varying amounts of polymer and fullerene detailed in Table III.1 are weighed out and placed in a glass vial along with 2 mL chlorobenzene and a magnetic spin bar. The active layer solution is left to stir overnight at 200 rpm on a hot plate set to 50° C. Once the solution is thoroughly mixed, it is run through a 0.45 μm PTFE filter to filter out any large

impurities. The photoactive layer is then spun on the substrate in a mechanical-type spin coating machine in the nitrogen glovebox. The slide is spun at varying terminal velocities for 60 seconds.

After the active layer has been deposited, the anode is cleaned again to expose the ITO anode, and the backside is cleaned as well. The sample is then loaded into a high-vacuum electron beam evaporating system and pumped down to at least the μTorr pressure range. 80 nm of aluminum is then deposited onto eight spots on the slide through the use of a shadow mask at a rate of approximately 1.0 Å/s. Lastly, the slide is removed from the vacuum chamber and is annealed at 150° C for 10 minutes in the nitrogen glove box.

The shadow masks for depositing aluminum are 1.7 mm in height and define the overall device structure; each cell is approximately 11 cm^2 in area. Figure III.1 shows the physical layout of the slide, including dimensions. To produce repeated trials, there are 8 total solar cells fabricated on each slide.

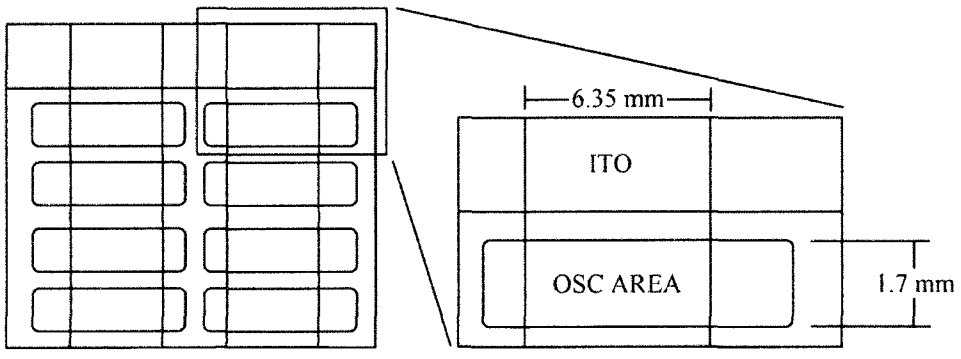

Figure III.1: Slide layout and OSC dimensions

III.3 Characterization Methods of Solar Cells

III.3.1 Current-Voltage Characterization

A current density (J) versus voltage (V) plot is an electrical characterization technique to determine properties of the OSC such as percent efficiency (PCE), fill factor (FF), and series and shunt resistances. To generate J-V plots, the solar cell is hooked up to a Keithley SourceMeter and placed under a Newport solar illuminator. The internal bulb and mirrors of the illuminator are adjusted to produce the most uniform and diffuse spot size, and the intensity is adjusted so that it is emitting the air mass (AM) 1.5 standard of 100 mW/cm^2, which is 1 sun. The voltage is swept from +1.0 down to -0.5 V, and the current is recorded.

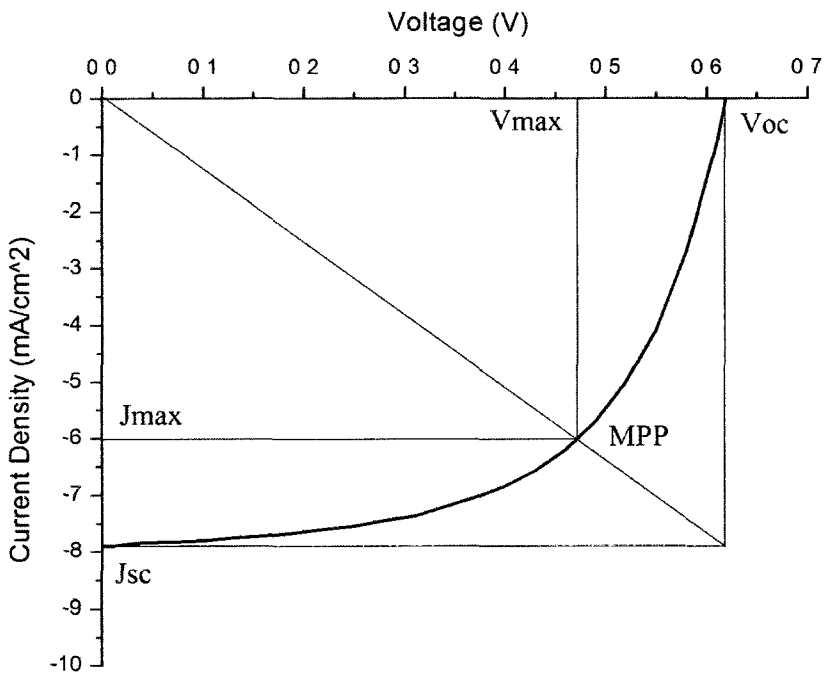

Figure III.2: Sample J-V curve with relevant electrical parameters

A sample output of a J-V plot is shown above in Figure III.2. On the graph, the current when V=0 is referred to as the short circuit current density (J_{SC}), and the voltage when J=0 is the open-circuit voltage (V_{OC}). The maximum power point (MPP) on the J-V curve is the point where the product of voltage and current density is the largest, and the corresponding voltage and current density of the MPP are referred to as V_{MAX} and J_{MAX}, respectively.

The FF is simply a ratio of the maximum power output of the cell to the product of V_{OC} and J_{SC}.

$$FF = \frac{MPP}{V_{OC}J_{SC}} = \frac{V_{MAX}J_{MAX}}{V_{OC}J_{SC}}$$

The PCE is the ability of the solar cell to convert solar energy to electrical energy and is a factor of the source irradiation (E) and the maximum power output by the solar cell.

$$PCE = \frac{MPP}{E} = \frac{FF \times V_{OC} \times J_{SC}}{E}$$

It is often useful to model a solar cell in terms of an equivalent circuit [57] to model the effects of power loss in the device, as shown in Figure III.3.

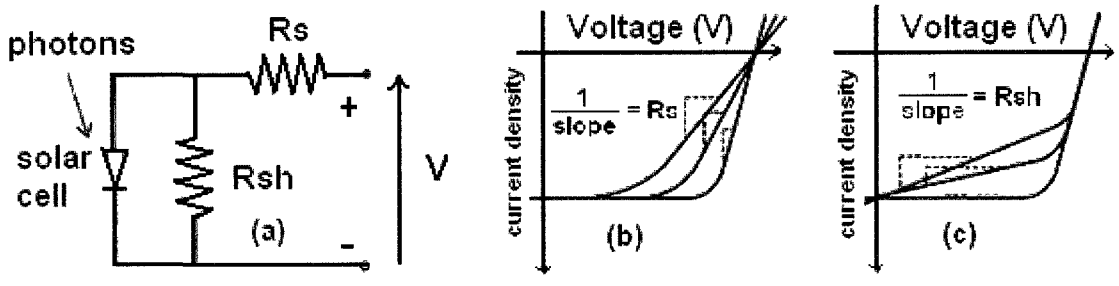

Figure III.3: (a) Solar cell equivalent circuit model, (b) calculation of series resistance, and (c) calculation of shunt resistance

The solar cell acts as a photodiode, and the two resistors model the shunt (R_{SH}) and series (R_S) resistances. For an ideal device, the shunt resistance would be infinite, and the series resistance would be 0, corresponding to 100% available power being dissipated across the photodiode; this would result in a 100% FF.

Since experimental devices do contain stray sources of power loss, it is important to model them. To estimate the shunt resistance, the inverse slope of the J-V curve is taken at the short circuit current density, and for the series resistance, the inverse slope of the J-V curve is taken at the open circuit voltage, as shown in Figure III.3.

In this study, current density-voltage characteristics will be used to determine the electrical properties of the devices such as PCE and FF, and the curves will also be analyzed to model the stray resistances in the device. The active layers which are used in the most efficient solar cells for each blend will be further analyzed with additional characterization techniques, which are detailed in sections III.3.2 to III.3.4.

III.3.2 Atomic Force Microscopy

Atomic force microscopy (AFM) is a physical characterization technique that images the surface of solid films with angstrom accuracy. For this study, the surface topology of the photoactive layer will be investigated by running AFM tests on the active layer spin casted onto a glass substrate. The glass substrates will be cut into 1 inch squares and cleaned using the same procedure as outlined in section III.2. The photoactive layer will be spin casted onto the substrate in the same fashion as fabricating solar cells.

The study at hand will be performed using a Dimension 3100 Scanning Probe Microscope and controlled by a Digital Instruments Multimode/Nanoscope III. The

substrate is placed on a piezoelectric device, and a cantilever spring with an ultra-fine tip oscillates in close proximity to the substrate. The AFM will be operating in tapping mode, which is when the tip of the spring is brought into intermittent contact with the sample. When the spring comes into close contact with the sample, it experiences the repulsive and attractive forces such as Van der Waals force and dipole interactions generated by the molecules of the film. The piezoelectric element of the device keeps the substrate at a fixed height above the spring, and a laser monitors the position of the spring. The feedback mechanisms in the system allow the sample to be kept at a fixed height above the substrate, and this deviation in height is converted to an output that shows the physical topography of the sample. The software not only generates 2-D and 3-dimensional (3-D) images of the surface, but it can also provide roughness measurements.

1 μm^2 areas of the substrates will be imaged by operating the machine at 0.5 Hz and 512 samples per line. Studying the physical structure of the active layer will provide insight as to why certain photoactive layer blends are more efficient than others in OSC applications. Visual inspection of each layer will be performed, and the roughness measurements will also be analyzed to determine trends in the active layers as the concentration of the film is increased.

III.3.3 Ultraviolet-Visible Spectrophotometry

Ultraviolet-Visible (UV-Vis) Spectrophotometry is an optical characterization technique that measures the absorption of a sample. Samples can either be tested in liquid form, or the measurements can be done for solid thin films. Since the interest is in the properties of the photoactive layer thin film, the measurements will be done on the

active layer spun on glass. The glass squares will be cut into one inch squares, cleaned using the same procedure as detailed in section III.2, and characterized with a Shimadzu 2401 UV-Vis recording spectrophotometer.

The absorption (A) of a sample is strongly dependent on the molar absorptivity (ε), concentration (c), and thickness (l) of the film, which is expressed by a derivation of the Beer-Lambert law, where $A = \varepsilon lc$. The absorption is a unit-less measurement that compares the intensity of the incident light to the light that has passed through the film. For absorption spectrum measurements, a sample of the photoactive layer film on glass is loaded into one holder, and a reference sample of plain glass is used as a reference, loaded in the other sample holder. The machine will sweep the wavelength of the light (and therefore energy) over the visible and into the UV-range, and the software will extract the absorption for each wavelength.

As stated earlier, a main drawback in polymer photovoltaics is the low absorption profile of the materials. This research proposes that by increasing the active layer density, the absorption profile of the blend will increase over the visible and UV wavelength ranges, which will lead to increased photocurrent density in the solar cells. Absorption of P3HT and PCBM films will be measured, as well as the photoactive layer films, to determine local absorption peaks and trends in optical performance.

III.3.4 Variable Angle Spectroscopic Ellipsometry

Spectroscopic ellipsometry (SE) is another optical characterization technique that is far more in-depth and valuable than simple absorption measurements. SE can be used to determine film thickness and other optical properties of a species such as the index of refraction (n) and the extinction coefficient (k).

SE operation begins with emitting an unpolarized light from a lamp source. The light is polarized in some fashion and then interacts with the substrate. The reflection of the light is further manipulated with another polarizer and collected with a photodetector or photodiode [58]. The software measures psi (Ψ) and delta (Δ) and manipulates electromagnetic equations to determine other properties of interest. Psi and delta are defined by $\tan(\Psi) = \frac{|R_S|}{|R_p|}$, where R_S and R_P are the incident and reflected wave amplitudes, respectively, and $\Delta = \delta_1 - \delta_2$, where δ_1 and δ_2 are the phase differences of the incident and reflected waves, respectively. These two parameters are related by $\rho = tan\Psi e^{j\Delta}$, where roe ($\rho$) is the complex reflectance ratio. The complex index of refraction, $\tilde{N} = n + jk$, is a variable in the equations for R_S and R_P [58,59].

To perform ellipsometry measurements, one square inch glass slides are cleaned using the standard cleaning procedure, and the photoactive layer is spun onto the glass. The measurements are taken at 4 different angles with a J. A. Woollam Variable Angle Spectroscopic Ellipsometer (VASE), with a wavelength distribution of 190-1690 nm. To fit the data, Cauchy's Equation is fit to the experimental data. Cauchy's Equation is given by $(\lambda) = A + \frac{B}{\lambda^2} + \frac{C}{\lambda^4} + \cdots$, where n is the refractive index, λ is the specific wavelength, and A, B, and C are constants that are varied to fit the data. The constants in Cauchy's Equation are modified as to limit the mean-square error in the data fitting [60]. All of this manipulation is done in the J. A. Woollam software WVASE32.

VASE will be done on P3HT, PCBM, and the photoactive layer thin films to determine their respective thicknesses and extinction coefficients. The extinction coefficient (k) is related to the absorption (A) of a sample by the absorption coefficient (α) outlined in the following equations.

$$A = \varepsilon lc \qquad A = \alpha l \qquad \alpha = \frac{4\pi k}{\lambda}$$

The profiles of the absorption and the extinction coefficient in the UV and visible range will both show how the intensity of light is affected when it interacts with the four photoactive layer films.

III.4 Conclusions

The experimental process begins with fabricating several planar structure organic solar cells under varying conditions. The composition of the photoactive layer will be varied, as well as the film thickness, to determine the optimal active layer for each blend. Once this has been determined, further characterization on the photoactive layer thin films will be performed to compare the electrical properties with the physical and optical properties. The PCE and FF, as well as stray resistances, will be calculated through electrical characterization techniques. To further understand the active layer structure, AFM measurements will be performed to compare the surface topology of the films. Also, UV-Vis absorption measurements will be done to compare the light intensity absorption of the active layers in the visible and UV ranges. Furthermore, VASE measurements will be performed to extract the thickness and the extinction coefficient of the films. Understanding these additional physical and optical characteristics of the photoactive layer films will provide insight as to why certain films outperform others electrically when integrated in an organic solar cell.

CHAPTER IV

ELECTRICAL PROPERTIES OF ORGANIC SOLAR CELLS

IV.1 Introduction

In this section of experimentation, the optimal photoactive layer processing parameters for the four blends under investigation were determined by comparing their PCE, and then four champion cells were made. For each active layer blend, four solar cells were fabricated, resulting in a total of sixteen unique solar cells. Among the four different cells for each blend, the only variable changed was the terminal spin speed of the active layer during spin casting, which was varied in the range of 750 up to 2000 rpm depending on the blend. Spinning the photoactive layer at different terminal velocities produced four unique thin films, with the most predictable difference being the layer thickness; lower spin speeds produce thicker films and higher spin speeds produce thinner active layers.

For the cells fabricated with the 20:16, 25:20, 30:24, and 35:28 blends, the application speed was varied between 750-1500 rpm, 1000-1750 rpm, 1000-1750 rpm, and 1250-2000 rpm, respectively, in increments of 250 rpm. The sixteen devices were fabricated in groups of 4 to keep experimental conditions constant among the cells; the four OSCs with the 20:16 blend were made simultaneously, the four OSCs with the 25:20 blend were made together, etc. The calculated PCE of the four cells made with each blend was compared to determine the optimal spin casting speed of the active layer, which is shown in Table IV.1. The P3HT:PCBM films were then spun at their optimal

conditions, and the active layer thicknesses were determined from SE measurements, which is also detailed in Table IV.1.

Table IV.1: Spin casting conditions for the four photoactive layer blends that produced the most efficient OSCs

Active Layer	Application Speed	Thickness
20:16	1000 rpm	55 nm
25:20	1250 rpm	70 nm
30:24	1500 rpm	77 nm
35:28	1750 rpm	88 nm

The results in Table IV.1 show that as the viscosity of the photoactive layer increases, the terminal spin casting speed must also increase. This trend is intuitive – the solutions that are more concentrated will need more angular velocity to spin off the required amount of material. Also, the layer thickness must increase as the material concentration of the active layer increases. The physical dynamics of the P3HT:PCBM film are more strongly detailed in Chapter V. Now that the optimal application conditions have been determined, the four champion solar cells (one with each active layer blend spun at the terminal velocities outlined in Table IV.1) will be characterized and analyzed.

IV.2 Results and Discussion

IV.2.1 Percent Efficiency and Fill Factor

The four champion OSCs were fabricated simultaneously to keep the experimental conditions constant among the cells. The J-V curves for the champion cells are displayed in Figures IV.1 and IV.2, and the data is compared in Table IV.2.

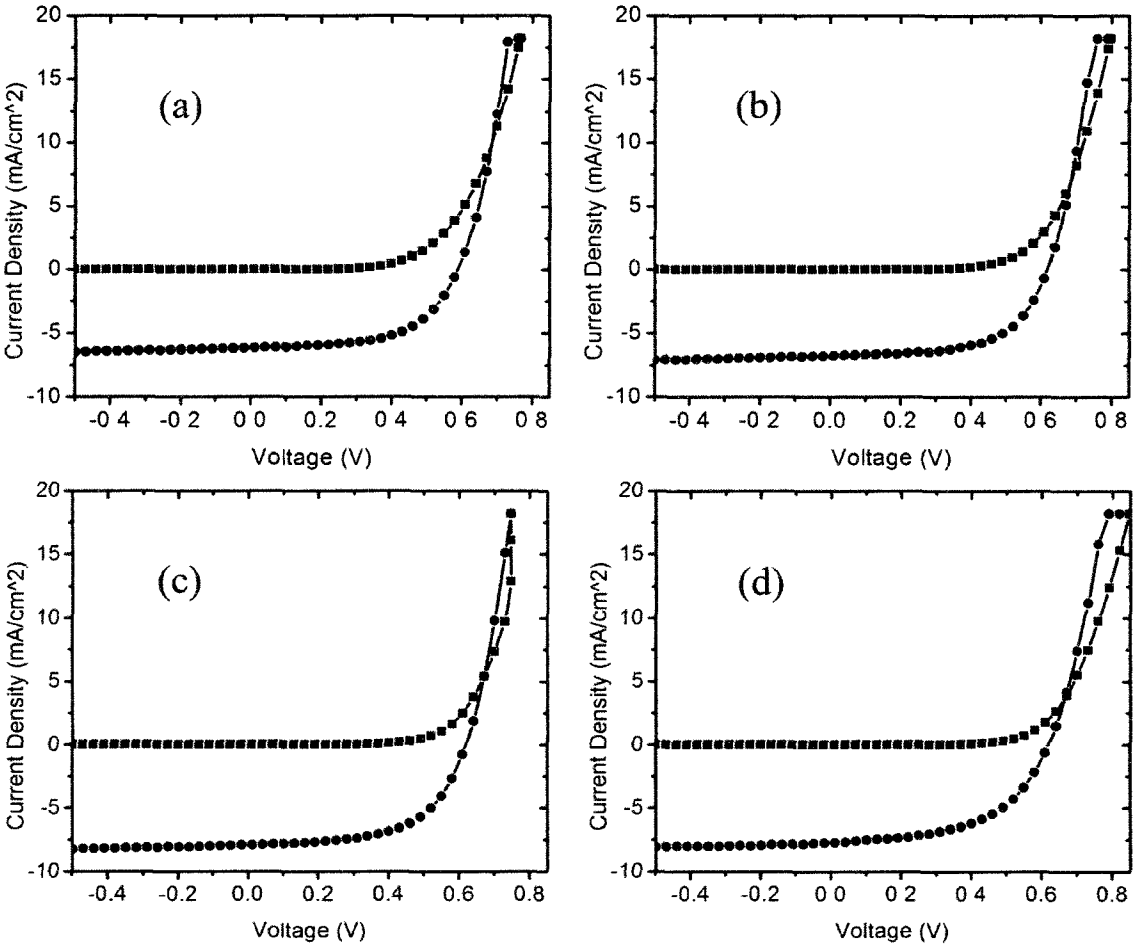

Figure IV.1: Light (●) and dark (■) J-V characterizations of the best solar cells fabricated with each photoactive layer blend: (a) 20:16, (b) 25:20, (c) 30:24, and (d) 35:28

Table IV.2: PCE, FF, V_{OC}, and J_{SC} of the four champion solar cells

Active layer	PCE	FF (%)	Voc (V)	Jsc (mA/cm^2)
20:16	2.11	58.4	0.590	6.16
25:20	2.51	60.0	0.618	6.78
30:24	2.86	58.6	0.619	7.89
35:28	2.54	53.4	0.618	7.69

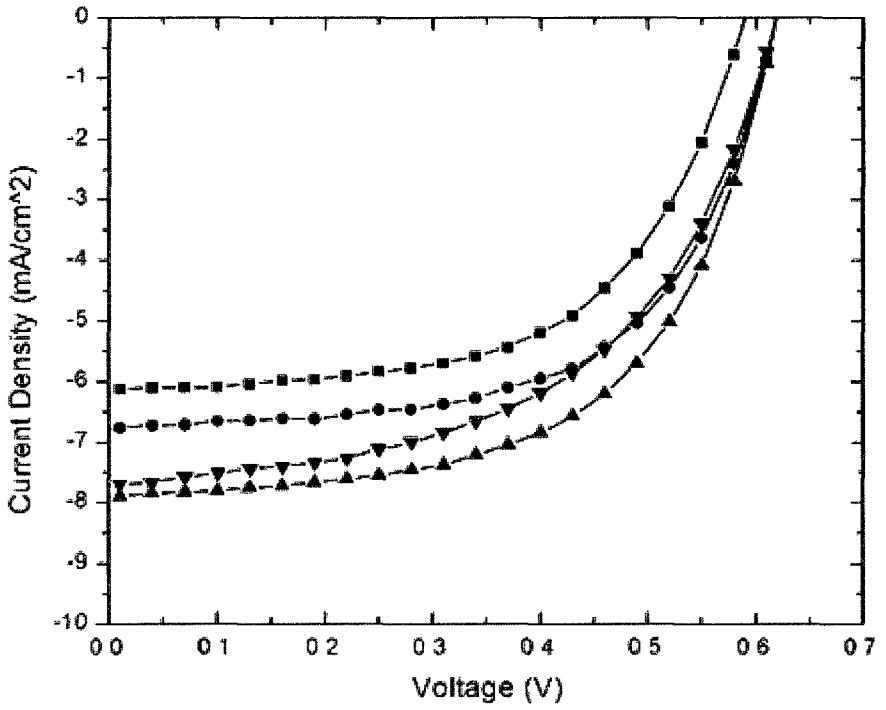

Figure IV.2: J-V characteristics of the most efficient cells from the four photoactive layer blends: ■(20:16), ●(25:20), ▲(30:24), and ▼(35:28), under 100 mW/cm^2 (1 sun)

From the data in Table IV.2 and Figures IV.1 and IV.2, it is concluded that an optimal photoactive layer density is crucial for maximum OSC device efficiency. The V_{OC} remains relatively constant throughout the devices since the V_{OC} depends mainly on the energy levels of the materials in the heterojunction and also the electrodes [61]. However, it appears that the PCE of the devices is directly related to the current density of the solar cells.

The efficiencies of the solar cells made with the 20:16 and 25:20 blends are 2.11 and 2.51, respectively. The general trends show that the less concentrated blends (20:16 and 25:20) provide a good fill factor (58.4% and 60.0%) yet lack the required current density (J_{SC} = 6.16 and 6.78 mA/cm^2) for a deep maximum power point. The smaller current densities among the solar cells fabricated with these solutions are due to

insufficient exciton generation in the heterojunction, possibly caused by the lack of absorption in the active layer. Since these layers are not densely packed and the FF remains high, recombination is ruled out as a reason for low current density.

The maximum PCE (2.86) among all four cells is achieved with the solar cell fabricated with the 30:24 photoactive layer blend. For the OSC made with this is active layer, the current density (J_{SC} = 7.89 mA/cm^2) is further increased, while the FF remains high (58.6%). The increased current density in the 30:24 solar cell is likely due to the strategic packing of the polymer-fullerene network. It is expected that a more concentrated blend would have enhanced self-organization of the donor-acceptor network, which would not only result in an increase in photon absorption but more fluid charge transport of the excitons through the heterojunction. The physical structure of the active layer will be further analyzed in Chapter V.

If the photoactive layer concentration is further increased, then the electrical properties of the cell start to decline. While the PCE (2.54) of the OSC made with the 35:28 blend is the second highest among the four cells, the FF (53.4%) sharply drops off. Also, the current density (J_{SC} = 7.69 mA/cm^2) begins to decrease rapidly compared to that of the cell made with the 30:24 blend. The lower current density and poor fill factor point toward recombination and leakage current losses in the photoactive layer. This is evident because in theory the absorption is at a maximum, which means that the amount of photo-generated excitons in the heterojunction is maximized. If the excitons were diffusing at the interfaces and being collected by the electrodes, then the current would be at a maximum, but it is apparent that charge recombination has thwarted this process.

IV.2.2 Stray Resistance Values

As described in section III.3.1, modeling a solar cell in terms of an equivalent circuit model can provide great insight to the loss mechanisms in the device. Furthermore, the stray resistance values can point toward sources of defects and imperfections in the cell structure, whether they be morphological or surface defects [57].

Table IV.3: PCE, FF, and the series and shunt resistance values for the four champion solar cells

Active layer	PCE	FF (%)	R-series (Ωcm^2)	R-shunt (Ωcm^2)
20:16	2.11	58.4	15.1	1440
25:20	2.51	60.0	12.2	1100
30:24	2.86	58.6	11.3	1110
35:28	2.54	53.4	14.4	630

Table IV.3 outlines the series and shunt resistance values of the champion solar cells made from each blend, which were determined by analyzing Figure IV.1. The PCE and FF are also listed in Table IV.3 as a comparison. It is clear that the series resistance values show the same trend as the PCE: improving resistance values from the 20:16 up to the 30:24 blend and then poor performance when the blend concentration exceeds 30:24. The shunt resistance values follow a slightly different trend; as the active layer density increases, the shunt resistance steadily decreases and is independent of device PCE.

The causes of stray resistance values in organic solar cells have been thoroughly outlined in the literature [57], and it is widely accepted that the series resistance plays a large role in OSC performance [30,57,62]. According to studies, the main factors that

influence the series resistance of cells are the intrinsic resistances associated with the cell and the active layer morphology [57]. Also, the active layer morphology is most heavily influenced by the post-fabrication annealing process, which causes the polymer to stack on the atomic level and the fullerene to aggregate in clusters [30, 57]. According to this thesis research, the series resistance, and more than likely the active layer morphology, is strongly influenced by the concentration of the active layer thin film.

The series resistance of the devices decreases from the 20:16 blend (15.1 Ωcm^2) to the 30:24 blend (11.3 Ωcm^2) and then increases in the 35:28 blend solar cell (14.4 Ωcm^2); this means that the morphology of the donor-acceptor network is probably optimal in the 30:24 photoactive layer blend and poorer for all others. For the less concentrated blends (20:16 and 25:20), the active layer morphology is probably not great due to the lack of material, resulting in less contact area among the donor-acceptor network. Conversely, the series resistance is also high for the 35:28 blend; the morphological defects in this layer are more than likely due to superfluous amounts of organics in the thin film, thereby increasing the series resistance and decreasing current density. All of this points toward the possibly that increasing the active layer density has some of the same effects on the donor-acceptor morphology as does thermal annealing; increasing thermal treatment up to a certain point improves device PCE and series resistance, but prolonged annealing leads to increasing series resistances and reduced device efficiencies [30].

It has also been determined that variations in shunt resistance result from impurities and defects in the active layer [57]. Possible sources of defects will be further

investigated in subsequent sections that characterize the physical nature of the active layer. For now, it is obvious that as the active layer concentration increases from the 20:16 blend up to the 35:28 blend, the shunt resistance steadily declines from 1440 Ωcm^2 down to 631 Ωcm^2. This leads to the conclusion that that the shunt resistance is heavily influenced by the density of the active layer thin film.

IV.3 Conclusions

In this section, the electrical properties of organic solar cells with various photoactive layer concentrations have been compared. It has been shown that the PCE of the devices is optimal when the 30:24 photoactive layer blend is implemented and is due in large part to the high short circuit current density and high fill factor, allowing for a deep maximum power point. Stray resistance values were also calculated, and it was determined that the series resistances of the devices follow a similar trend as the PCE, whereas the lowest series resistance value belonged to the cell fabricated with the 30:24 blend. This points towards the morphology of the donor-acceptor network being optimal inside of the 30:24 blend, allowing for smooth and efficient charge transport. The literature widely agrees that the crystalline network of polymer and fullerene in the active layer decreases series resistance and improves overall device performance [30,54]. In the subsequent chapters of this research, the physical and optical properties of the active layer will be examined to provide justification for the obtained electrical properties in this chapter.

CHAPTER V

PHYSICAL PROPERTIES OF P3HT:PCBM THIN FILMS

V.1 Introduction

In the previous chapter, the OSCs with four different photoactive layer blends were characterized to determine their electrical properties. This chapter will provide insight to the physical structure of the four P3HT:PCBM films that were used to fabricate the solar cells in Chapter IV. AFM measurements will be done on one square micrometer areas of the annealed P3HT:PCBM thin films to observe the nanoscale morphology of the surface of the active layers.

It is well known that the nanoscale morphology of the photoactive layer surface influences the physical operation of polymeric solar cells [20,29]. The lateral surface profile obtained by AFM measurements provides indicative insight to the bulk morphology of the organic layer. Overall, the 3-D network morphology is the most important factor when characterizing the physical properties of the photoactive layer [29,65]. Studies report that thermal annealing of the photoactive layer produces a crystalline 3-D network of donors and acceptors, with the P3HT stacking in a lamellar fashion, and fullerene diffusing to nucleation sites throughout the active layer [20,28,30]. The enhanced crystallinity, verified through tunneling electron microscopy (TEM) and X-ray diffraction (XRD), induces favorable molecular packing, creating more interfacial area among donors and acceptors in the photoactive layer [29,30].

V.2 Results and Discussion

The four photoactive layers under investigation were spun at their optimal spin speeds on cleaned glass and subsequently annealed in the nitrogen glove box for ten minutes at 150° C. To observe the topology of the top surface of the active layers, the samples were characterized under AFM. To investigate the effects of thermal annealing on active layer morphology, Figure V.1 on the following page shows AFM images for un-annealed (a) and annealed (b) 30:24 active layer. Based on the AFM images, it is clear that for the un-annealed sample, the overall surface roughness (RMS roughness = 0.501 nm) is much smoother than the sample that received thermal treatment (RMS roughness = 0.841 nm). The annealed active layer film shows deeper valleys and higher peaks on the AFM images, which is an indication of enhanced crystallinity of the P3HT:PCBM network [30,32,54]. Increased crystallinity in the active layer not only enhances the molecular stacking of the organics [20,30] but also leads to a greater surface area for the organic-cathode interface, which has been shown to enhance the absorption of the cells [20,32,51,65] and the electrical properties of the devices such as charge mobility [39,51] and PCE [30,64,55].

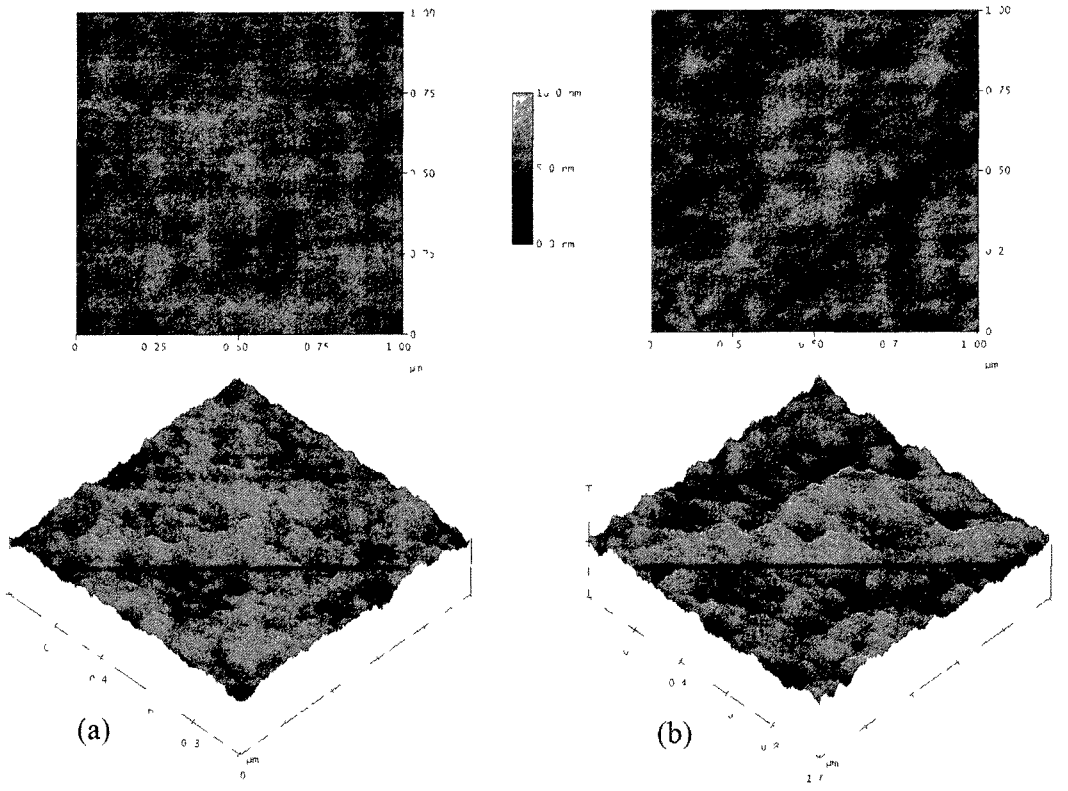

Figure V.1: (a) Pristine and (b) annealed (150° C for 10 minutes) films of 30:24 P3HT:PCBM films on glass

Next, the four photoactive layer blends (20:16, 25:20. 30:24, and 35:28) were spun at their conditions yielding the highest efficiencies at their respective concentrations on glass substrates and also annealed with the aforementioned conditions. The 2-D and 3-D images of the top of the films are shown on the next page in Figures V.2 through V.5, and their roughness measurements are detailed in Table V.1.

Table V.1: RMS roughness of the annealed P3HT:PCBM films

Active Layer	RMS Roughness
20:16	0.757 nm
25:20	0.801 nm
30:24	0.841 nm
35:28	0.927 nm

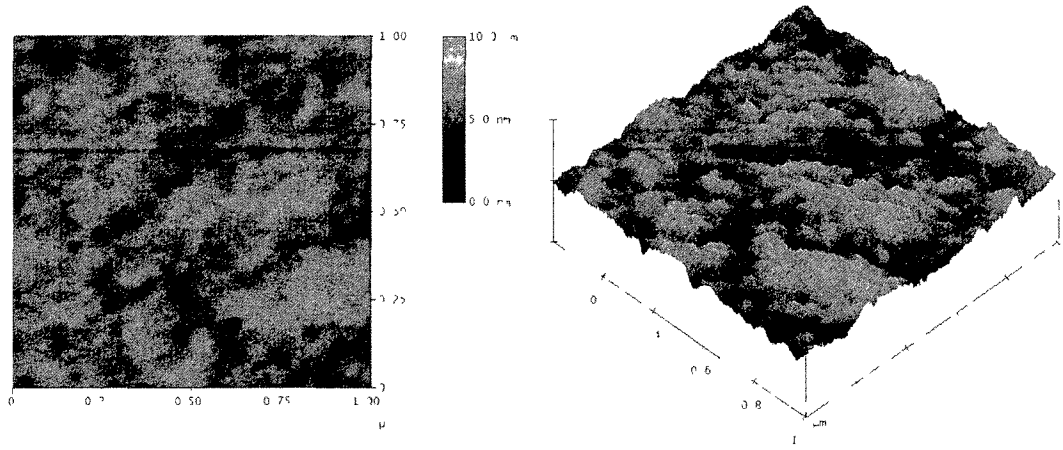

Figure V.2: 2-D and 3-D AFM images of 20:16 P3HT:PCBM

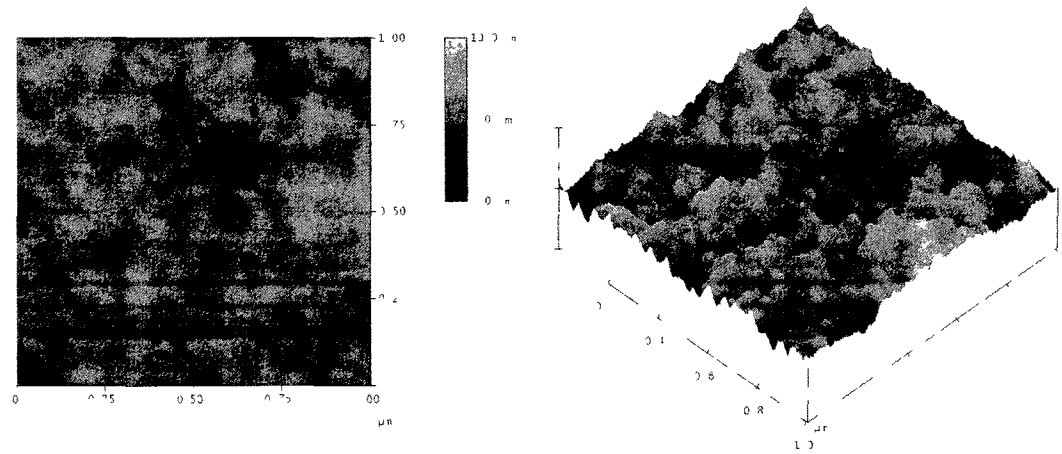

Figure V.3: 2-D and 3-D AFM images of 25:20 P3HT:PCBM

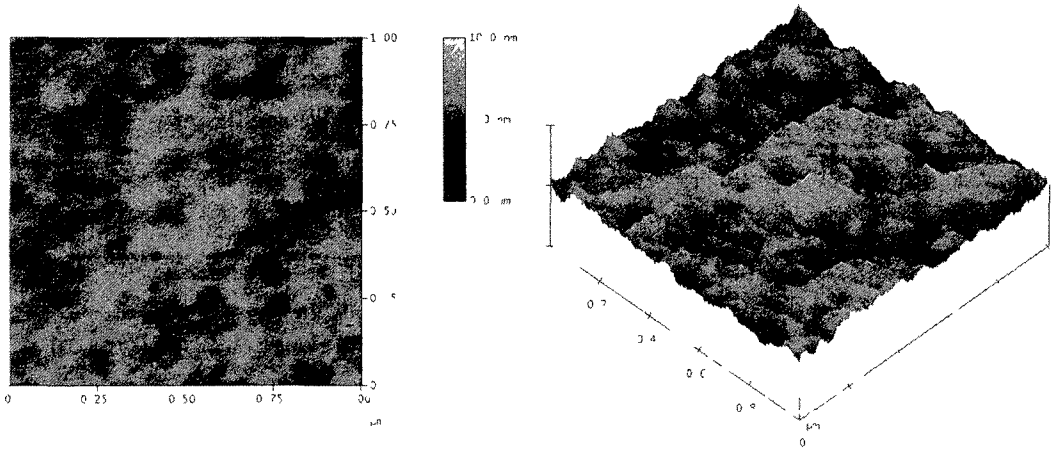

Figure V.4: 2-D and 3-D AFM images of 30:24 P3HT:PCBM

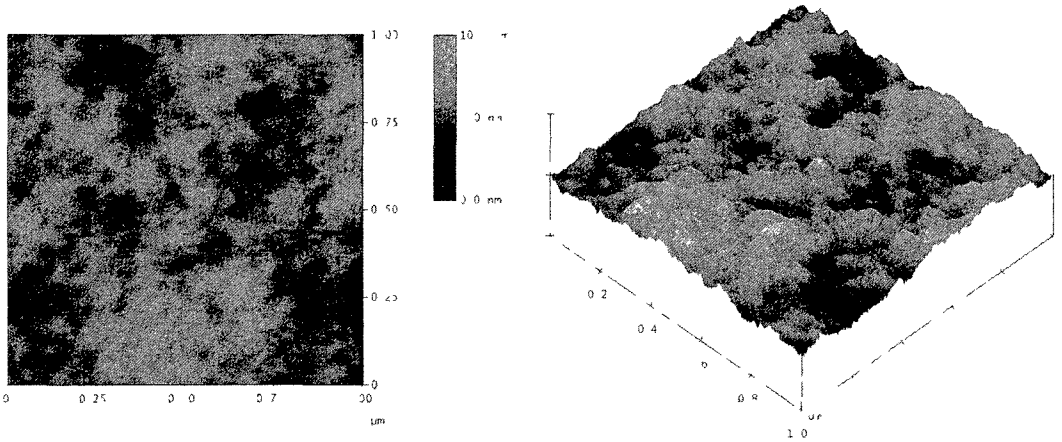

Figure V.5: 2-D and 3-D AFM images of 35:28 P3HT:PCBM

Based on Figures V.2 through V.5, there is an increasing trend in roughness as the concentration of the P3HT:PCBM thin film increases. The 20:16, 25:20, 30:24, and 35:28 blends increase in RMS roughness from 0.757, 0.801, 0.841, and 0.927 nm, respectively. The increasing RMS roughness of the thin films directly corresponds to the amount of organics in the layer, and the increasing thicknesses of the layers. When there is more P3HT and PCBM in the thin film, the thickness of the structures increase, and the deviating morphology of the active layer surface increases accordingly.

With respect to P3HT:PCBM annealing, increasing values of RMS roughness are advantageous in bulk heterojunction OSCs because they are an indication of enhanced donor-acceptor contact area and an improved contact layer between the cathode and the photoactive layer [30,32]. However, since all of these active layers are annealed, it is unclear as to what effect increasing the active layer concentration has on the overall morphology of BHJ polymer solar cells. It is apparent that as the active layer density increases, the RMS surface roughness increases, but it is unclear as to what effect this has on the 3-D physical structure, and the solar cell performance. As shown in Table V.1, the increase in RMS roughness from 0.757 nm up to 0.927 nm is miniscule; angstrom-level variations in topology might not have a profound impact on device performance.

It is known that the series resistance of an OSC depends primarily on the thickness and 3-D morphology of the P3HT:PCBM layer, and the shunt resistance depends on the presence of defects or impurities in the active area that could cause recombination and leakage current [57]. Referring back to Table IV.3, the series resistances steadily decrease to 11.3 Ωcm^2 in the 30:24 P3HT:PCBM layer and then increase again in the 35:28 blend. The shunt resistance of the devices steadily drops from 1440 Ωcm^2 down to 630 Ωcm^2 when the active layer density is increased from the 20:16 blend up to the 35:28 blend. The RMS surface roughness of the P3HT:PCBM thin films does steadily increase from 0.757 to 0.927 nm, but these sub-angstrom deviations alone cannot explain the electrical properties of the cell.

V.3 Conclusions

The physical structure of the photoactive layer has been thoroughly investigated by conducting AFM measurements. The 2-D and 3-D surface images show that increasing the density of the P3HT:PCBM layer causes a slight increase in the RMS roughness of the active layer thin film as shown in Figure V.6.

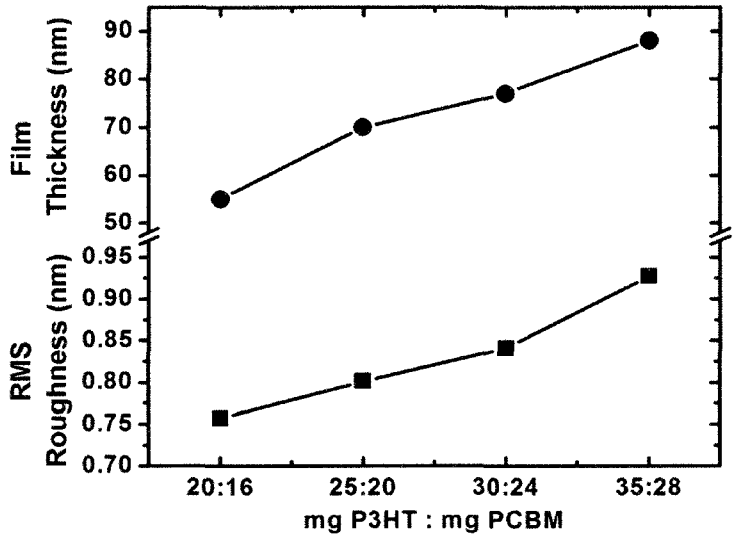

Figure V.6: RMS roughness and film thickness of each photoactive layer

When attributing increased roughness to thermal annealing, it is advantageous because it is an indication of enhanced crystallinity of the donor-acceptor network. However, all of these samples have received thermal treatment; therefore, the angstrom-level deviations alone cannot conclusively explain the deviating electrical properties of the OSCs under investigation.

CHAPTER VI

OPTICAL PROPERTIES OF P3HT:PCBM THIN FILMS

VI.1 Introduction

Thus far, the electrical properties of the organic solar cells have been compared, and the physical properties of the P3HT:PCBM thin films used in the OSCs have been characterized. This chapter will explore the optical properties possessed by the various photoactive layers of P3HT:PCBM, including the absorption and extinction coefficients over an appropriate spectral distribution. The absorption of the thin films was determined by doing ultraviolet-visible (UV-Vis) spectrophotometry on the annealed thin films of P3HT, PCBM, and the four unique blends of P3HT and PCBM that were incorporated into the OSCs. For determining the extinction coefficients, VASE was implemented on the exact same samples that were used for UV-Vis characterizations.

There are several factors that can affect the absorption of P3HT:PCBM thin films; most notably, the Beer-Lambert law equates the absorption to the product of molar absorptivity, material concentration, and film thickness. Molar absorptivity is an intrinsic property, the material concentration is obviously dependent on which photoactive layer is tested, and the thickness will also vary among the active layer thin films. Since the product of these factors determines the absorption, one would expect that the absorption would increase if the photoactive layer concentration increases since the material concentration and film thickness are steadily increasing from the 20:16 blend up to the 35:28 blend. Absorption in P3HT:PCBM thin films is important because if the degree of absorption is higher, then more electron-hole pairs are being generated;

if more excitons are present in the active layer, then the current density in the solar cells will also increase.

The extinction coefficient of the photoactive layers is another important optical property and is closely related to the absorption of the film. Further manipulation of the Beer-Lambert law shows that absorption can be expressed in terms of an absorption coefficient; the absorption coefficient is also dependent upon the extinction coefficient of the material. If the absorption loss when light passes through the medium is higher (larger values of k), then this is another indication that the incoming photons are stimulating the polymer and fullerene, thereby creating more excitons and subsequently current, given efficient charge separation. It is expected that the peaks of k will lie in the same region as the peaks of absorption. In the literature, studies have been done on the complex index of refraction of individual P3HT and PCBM thin films but not many studies in which k has been explored for various photoactive layers, as done in this research.

It is crucial that the photoactive layers maximize the usage of incoming light. In organic semiconductor technology, it is common to have absorption peaks in the visible and UV range, and little to no absorption the infrared region [36]. This is inherently problematic in OPV technology since such large energies are required to generate excitons. Furthermore, the peak irradiation of the air mass 1.5 spectrum occurs around 500-700 nm (2.48-1.77 eV) [36,66], with the overwhelming majority of the spectral irradiance lying in the infrared region and little irradiation occurring with wavelengths less than 700 nm. Figure VI.1 shows the irradiance distribution over a wide spectral range according to the standard AM 1.5 [66]. The high energy bandgap of organic

semiconductors such as P3HT and PCBM leads to severely mismatched spectral distributions; photogenerated excitons in the polymer and fullerene require photon energies from the visible or ultraviolet spectrum, yet the vast majority of the AM 1.5 irradiance occurs in the infrared region.

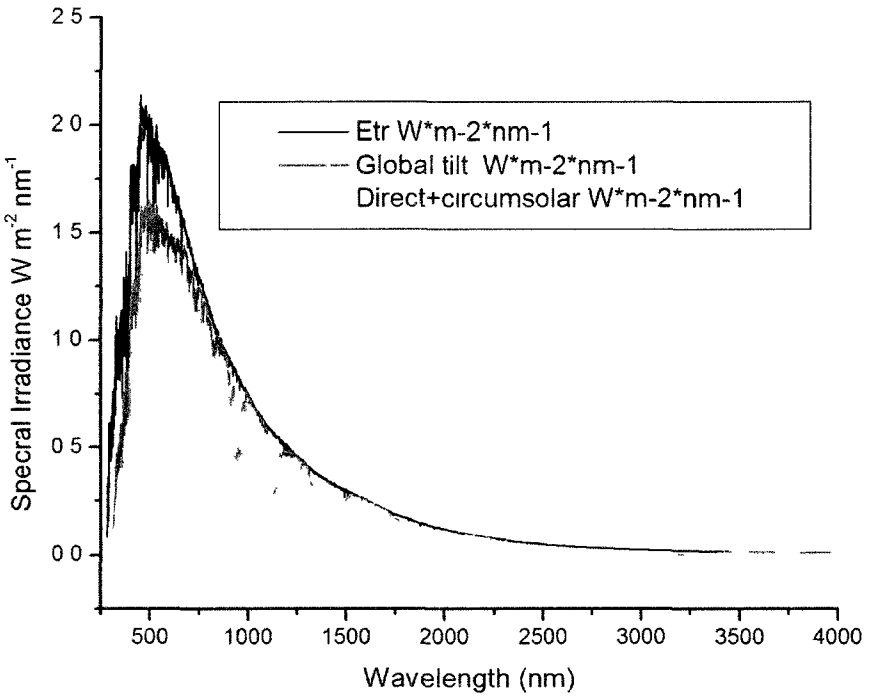

Figure VI.1: Distribution of spectral irradiation according to ASTM; etr (extraterrestrial) and global tilt are provided for reference, and direct+circumsolar is AM1.5, and is used when characterizing solar cells [68]

Therefore, it is of utmost importance in polymer photovoltaics to maximize the optical properties of the photoactive layer materials. If the absorption, indices of refraction, and extinction coefficients of the photoactive layers are optimized, then the devices will generate more excitons and have a greater chance of generating large currents.

VI.2 Results and Discussion

VI.2.1 Absorption Spectrum

The absorption of a thin film is simply a measure of the change in light intensity when photons are passed through a sample. The local peaks are an indication of the required energy to excite an electron from the (HOMO) to any of the outer, unoccupied orbitals (LUMO) [71]. For typical conjugated polymers, the required energy to raise an electron from the HOMO to the LUMO, the bandgap energy, is fairly high; the energy band gap for P3HT is approximately 1.9 eV, and that of PCBM is about 2.4 eV [46]. To estimate the minimum required energy to excite an electron in P3HT or PCBM, the equation $E_g = hc/\lambda$ is used, where E_g is the bandgap energy, h is Planck's constant, c is the speed of light in a vacuum, and λ is the photon wavelength. To generate an exciton in P3HT, the light should have a maximum wavelength of approximately 650 nm, and for PCBM, photons can have a maximum wavelength of about 515 nm. To investigate this, Figure VI.2 shows the absorption spectrum of annealed P3HT and PCBM films.

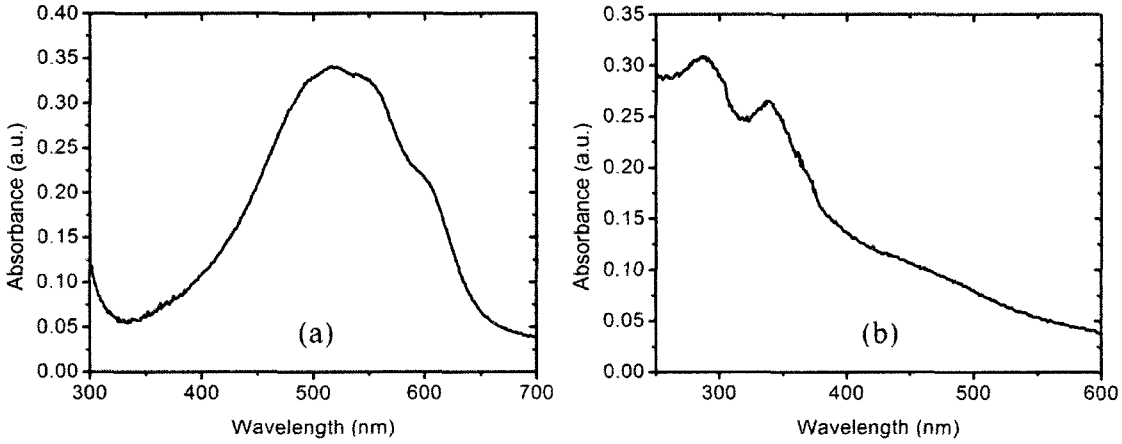

Figure VI.2: Absorption spectrum of annealed films of (a) P3HT and (b) PCBM

Figure VI.2 (a) contains the absorption spectrum for P3HT, and it shows three distinct relative maximum points of absorption. These three points occur at photon wavelengths of ~515, ~540, and ~605 nm. The PCBM, shown in Figure VI.2 (b), has two maximum points at ~290 and ~340 nm, and a soft shoulder in the range of 475 to 500 nm. All of these peaks are at higher energy wavelengths than the required wavelengths previously calculated (650 nm for P3HT and 515 nm for PCBM) to generate an exciton. The P3HT has absorption peaks at lower-energy wavelengths and the irradiance spectrum of air mass 1.5 is mainly in the visible and infrared range; this shows that the exciton generation in polymer-fullerene BHJ solar cells is dominated by P3HT, and the PCBM does not have as large a role in electron-hole formation.

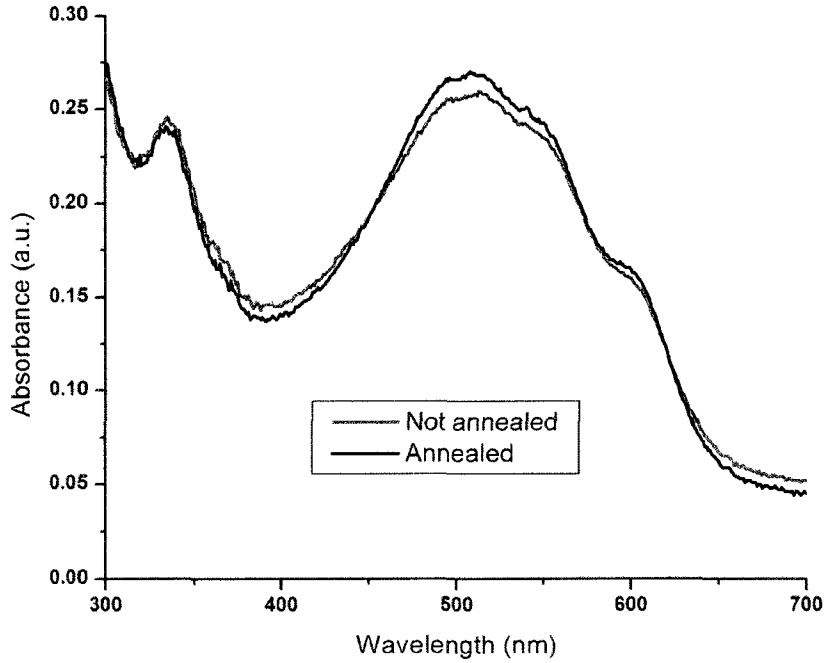

Figure VI.3: Absorption spectrum of 30:24 P3HT:PCBM thin films with and without thermal annealing (10 minutes at 150° C)

It has been reported [41,42] that increasing the purity of the organics, maximizing the regioregularity of the P3HT, and thermal treatment of the photoactive layer blend of P3HT and PCBM will positively impact the absorption profile by increasing the absorption peaks and slightly driving the peaks towards the infrared region. To show the effects of thermal annealing on the absorption profile, Figure VI.3 shows P3HT:PCBM thin films with no treatment and with thermal annealing.

Based on Figure VI.3, it is clear that when the blend of P3HT and PCBM receives annealing treatment, the peaks in the visible range slightly increase but not by a significant amount. While thermal treatment enhances the structural and electrical properties of the devices, it appears that annealing does not significantly impact the optical absorption of the photoactive layer films. Figure VI.3 is also useful because it shows the relative maximum points of absorption that are influenced by both the polymer and fullerene. There is one local peak in the UV range at ~330 nm, influenced by the PCBM in the blend, and three peaks exist in the visible range at ~510, ~555, and ~605 nm, due to the presence of P3HT. These peaks are very consistent with published research [32,67], which also shows the absorption peaking in those exact same ranges.

Since annealing doesn't have a profound impact on the absorption, further investigation must be done on other active layer treatments to increase the absorption of the photoactive layer films. Figure VI.4 on the following page shows the absorption of the four photoactive layer films that were used in this investigation, each with varying concentrations.

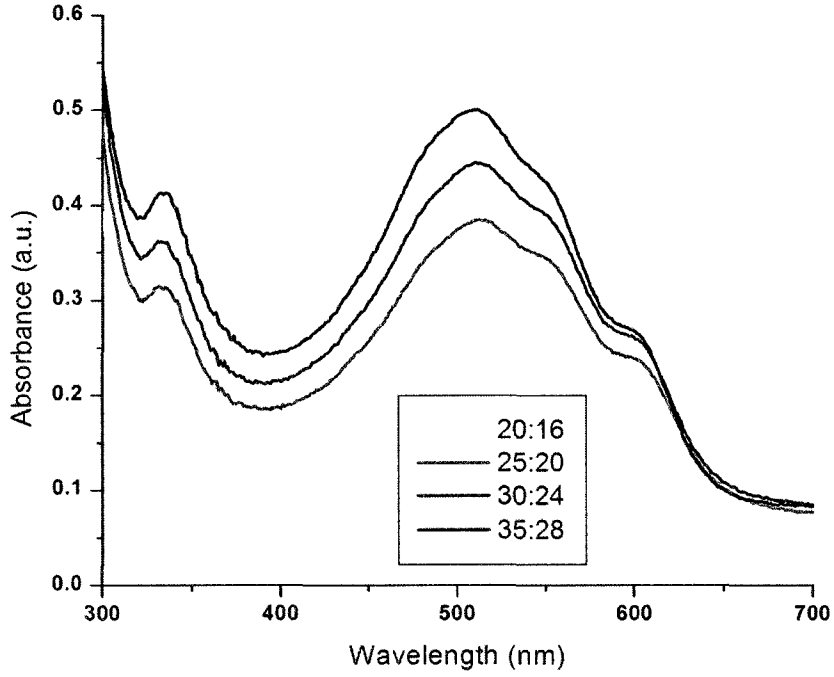

Figure VI.4: Absorption spectrum of the four photoactive layer blends that have been annealed for 10 minutes at 150° C

It is clear that as the concentration of the P3HT:PCBM film increases, the absorption of the photoactive layer increases also. This trend is expected given the Beer-Lambert law with the known information about the photoactive layer films. The absorption of the thin films depends on the product of molar concentration and film thickness; as the density of the photoactive layers increases from 36, 45, 54, up to 63 mg/2mL, the solid film thicknesses increase from 55, 70, 77, up to 88 nm, respectively.

VI.2.2 Extinction Coefficient

Another optical measurement that is important in understanding OPV devices is the extraction of the extinction coefficient (k) of the photoactive layers, which is the imaginary term in the complex index of refraction ($\tilde{N}$). The real term, n, is a measure of how much the speed of light slows down when passed through a material. k, on the other hand, is a measure of absorption loss when light travels through a medium. It is

expected that these two parameters will closely reflect the absorption spectrum measurements obtained in the previous section. Figure VI.5 shows the values of k for the individual films of P3HT and PCBM, which have been annealed for 10 minutes at 150° C.

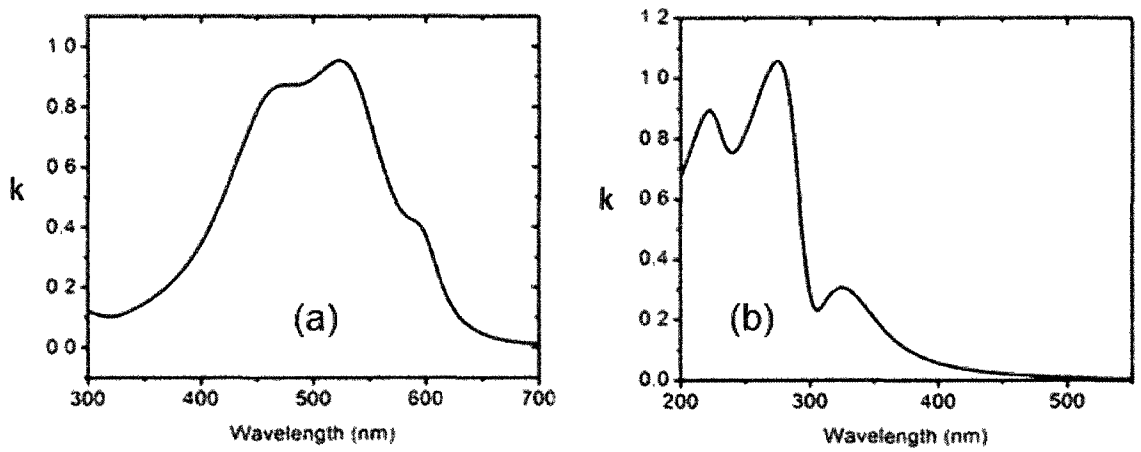

Figure VI.5: k for annealed films of (a) P3HT and (b) PCBM

Based on Figure VI.5, the local peaks of k for both P3HT and PCBM lie in the same range as their respective absorption peaks. P3HT contains local maximums of k at ~475, ~525, and ~595 nm. PCBM shows local peaks of k at ~220, ~275, and ~325 nm. The local maximum values of k for P3HT lie in the spectral range of 475-600 nm, which is the same range as the peaks of absorption, referring back to Figure VI.2. For PCBM, the local peaks of k occur between 220-325 nm, which is also the same region where the PCBM absorption peaks are present. Furthermore, based on the studies that have been done that examine the complex index of refraction for individual P3HT and PCBM films [68], the local peaks of the extinction coefficient for both the polymer and fullerene are in a range that is consistent with the literature.

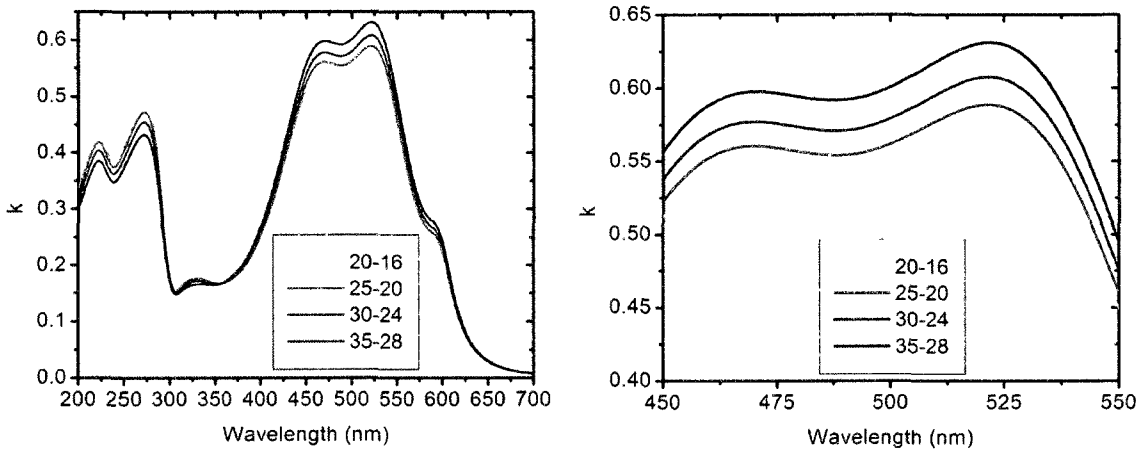

Figure VI.6: k values for the four photoactive layer blends

To investigate the extinction coefficient of the four photoactive layers, k was extracted from the SE data, and is displayed in Figures VI.7 and VI.8. It is clear that as the concentration of the photoactive layer increases, the dominant peaks influenced by the P3HT increase in magnitude as well; this trend is identical to the trend observed from the absorption spectrum measurements. All of the blends have peaks of k at ~470 and ~520 nm, which are consistent with published research reports [69,70,71].

VI.2.3 Discussion

As discussed earlier, the spectral mismatch of organic semiconductors is severe due to the relatively high energy band gaps of the materials [36]. This is also clear based on the results obtained in the previous section. For the spectrums of absorption and extinction coefficient for the photoactive layer blends, the local peaks of these parameters all occur in the visible and UV ranges; this is limiting since the irradiance distribution of AM 1.5 is almost entirely in the infrared region. Unfortunately, the peak values of the observed optical properties cannot be shifted into the infrared region unless different materials are chosen with lower band gap energies. Therefore, the optical

properties of the P3HT:PCBM photoactive layer must be optimized to try to maximize the usage of the photons in the visible spectrum near the infrared range.

From the absorption spectrum data in Figure VI.4, it is clear that as the photoactive layer concentration increases, the absorption over a wide spectral distribution increases as well. Similar trends are observed for the extinction coefficient; as the concentration of the four photoactive layers increases, the peaks in the visible region for k increase as well. However, the trend is opposite for the spectrum of k in the UV range; the peaks of k decrease as the photoactive layer density increases. As stated previously, the majority of irradiation in the standard AM 1.5 occurs in the visible and infrared regions, so the peaks in the UV range are not very influential to overall device characteristics and are not normally reported in publications [69,70,71].

The trends of absorption and extinction coefficient are critical to OSC performance. If the absorption and k in the photoactive layers are increased, this means that an increased amount of photons are exciting the P3HT:PCBM layer. As a direct result, the amount of photogenerated excitons will increase in the photoactive layer. If more excitons are present in the photoactive layer, then there is a greater chance that more charges will dissociate to the donor-acceptor interfaces and traverse the layers of the cell to generate current.

These properties also serve as an indication of the physical 3-D morphology of the photoactive layer. Several studies have been done [73,74] in which the optical properties, such as absorption spectrum, are compared with other characterization techniques such as XRD and AFM. It has been shown that while the roughness of a sample increases, the absorption increases as well; furthermore, the peaks of diffraction

increase as well, which all serve as in indication that there are larger crystallites in the photoactive layer, which is inherently advantageous in BHJ solar cells.

As all of the peaks of the investigated optical properties increase, the current density of the solar cells increase as well, up to a certain point. For the 20:16, 25:20, and 30:24 solar cells, the short circuit current density steadily increases from 6.74, 7.44, up to 8.67 mA/cm^2, which is a clear indication that increasing absorption and extinction coefficient lead to enhanced current density. Since the 35:28 photoactive layer has the largest peaks for all of the optical properties under investigation and also has the largest RMS roughness, it is likely that the 35:28 film has the highest degree of crystallinity, and therefore the most excitons being generated in the layer. However, the electrical performance of the 35:28 OSC is plagued due to the decreased current density (J_{SC} = 0.848) and low shunt resistance (R_{SH} = 630 Ωcm^2). This is possibly due to recombination in the active layer or leakage current [58]. The solar cell made with the 30:24 photoactive layer has the highest PCE because the absorption and extinction coefficient peaks are very high, while the stray resistances remain low.

VI.3 Conclusions

In this chapter, the optical qualities of the four photoactive layer films were under investigation. Absorption measurements were done on the photoactive layers, and it was observed that the peaks of absorption increased in magnitude as the concentration of the layers increased. For the extinction coefficient of the films, the peaks in the visible spectrum increased as the photoactive layer density increased, but the peaks in the UV range decreased as the layer increased in concentration. Because the vast

majority of solar irradiation is in the visible and infrared range, the peaks in the UV range do not play a very large part in overall device performance. These trends are evident when compared to the electrical properties of the cells; increasing peaks of these optical properties correspond to increasing current density in the cells, up to the 30:24 blend. This trend is broken in the 35:28 photoactive layer because this film suffers from stray resistances, which are a sign of recombination in the donor-acceptor network [57].

CHAPTER VII

SUMMARY AND FUTURE WORK

VII.1 Summary of Research

Throughout this study, the electrical, physical, and optical properties of planar-structured organic solar cells were explored, while altering the material concentration of P3HT and PCBM in the photoactive layer. Several solar cells were fabricated, and the optimal electrical characteristics were observed when the photoactive layer was made from a solution consisting of 30 mg P3HT and 24 mg PCBM dissolved in 2 mL chlorobenzene. The cells with less concentrated photoactive layers lacked sufficient current density, but if the P3HT:PCBM layer was too dense, then the cells suffered from recombination, severe degradation of the shunt resistance, and decreased current density.

Structural analysis was done on the four unique P3HT:PCBM blends, and it was observed that the RMS roughness of the photoactive layers linearly increased as the concentration of the blends increased and also as the film thickness increased. RMS roughness is a desired property when attributed to annealing the active layer because it is an indication that the 3-D morphology is more crystalline in nature. Since all four photoactive layers were annealed, it is unclear what effect increasing the concentration of the active layer has on the bulk 3-D morphology of the donor-acceptor network.

Lastly, the optical properties of the photoactive layers were investigated as well. The absorption and extinction coefficient were both extracted over a wavelength spectrum in the visible and UV ranges. All of these optical properties showed increasing peaks in the visible region as the photoactive layer concentration increased.

As the amount of organics in the thin film increased, the photons had more molecules and electrons to stimulate, generating more excitons. Subsequently, enhanced current density was observed in the devices fabricated with more concentrated photoactive layers. The 35:28 blend did have the maximum peaks of absorption and extinction coefficient, but the recombination in the layer, evident by the stray resistance values, prohibited that photoactive layer from efficiently dissociating the electron-hole pairs.

VII.2 Future Work

The structure of organic solar cells fabricated in this research (ITO/PEDOT:PSS/P3HT:PCBM/Al) currently serve as a reference or a base for emerging solar cells technologies. Most modern research OSCs contain interfacial buffer layers that serve as either a charge blocker or charge transporting agent. For example, other studies show that the fullerene tends to settle at the bottom of the photoactive layer [52]. This problem is being addressed by incorporating a film of P3HT sandwiched between the PEDOT:PSS layer and the bulk heterojunction P3HT:PCBM photoactive layer [75], which enhances the electron blocking capabilities of the PEDOT:PSS layer and improves the optical and electrical properties of the cells.

To further enhance the charge transport in polymer-fullerene solar cells, interfacial metal oxide layers are being implemented into the device. The transparent oxides have been implemented between the PEDOT:PSS and P3HT:PCBM donor-acceptor network [75,76] and between the photoactive layer and the cathode [31]. All of these techniques enhance the charge transport in the devices, which is evident through improved fill factor and PCE.

Currently, work is being done on tandem solar cell structures, in which two individual layers of PEDOT:PSS/polymer:fullerene/TiO_x are sandwiched between the ITO and aluminum [24]. In these structures, the two polymer:fullerene photoactive layers are different; one of them will be the classical P3HT:$PC_{61}BM$ heterojunction, as detailed in this thesis study, and the other will incorporate a new low-bandgap polymer such as PCPDTBT [77] or PCDTBT [78]. These lower-bandgap polymers are advantageous because they can harvest solar irradiation deeper into the infrared region, while the P3HT absorption drops to 0 at wavelengths of ~650 nm. When the tandem structures are implemented, one polymer:fullerene layer consists of the traditional P3HT:PCBM blend, which has absorption peaks in the visible range. The other cell in the tandem structure uses a blend of lower-bandgap polymer and fullerene, such as PCPDTBT:PCBM, which has local peaks of absorption in the wavelength range of 750-800 nm [79]. The two distinct photoactive layer blends, when used together, can harvest a very wide range of irradiation; also, the titanium oxide spacers enhance the open circuit voltage of the devices [78], which will greatly increase the maximum power point of the devices.

VII.3 Importance of Thesis Work

The volatility of the global energy market, as well as the increasing evidence of global warming, have emphasized the need for a clean, renewable form of energy to supplement the current energy portfolio [6,7,8]. Organic solar cell technology is far from being a market force due to the relatively low device efficiencies and instability in ambient air [25,26]. However, the flexibility of polymer chemistry and device structures

show great promise for the technology [18]. Currently, P3HT:PCBM solar cells are being used as a base or a reference to produce the next generation of solar cells with interfacial layers [31,74,75,76] and tandem structures that utilize lower-bandgap polymers [24,77,78,79]. In order to maximize the efficiencies of these novel structures, every aspect of the device must be optimized. One of the most important and also volatile layers of the organic solar cells is the polymer-fullerene bulk heterojunction. In order for the entire device to function efficiently, the photoactive layer has to be optimized. In this study, the photoactive layer of P3HT:PCBM was optimized by increasing the material concentration of polymer and fullerene while keeping the weight ratio of the organics constant prior to deposition. This will set the groundwork for the next generation of polymer photovoltaics.

REFERENCES

[1] A. Shah, P. Torres, R. Tscharner, N. Wyrsch, and H. Keppner, "Photovoltaic technology: the case for thin-film solar cells," *Science*, vol. 285, no. 5428, pp. 692-698, July 1999.

[2] R. Ohl, "Light-sensitive electric device including silicon," U.S. Patent 2 443 542, 15 June, 1946.

[3] J. Mandelkorn, "Fabrication and characteristics of phorphorous-diffused silicon solar cells," *Journal of the Electrochemical Society*, vol. 109, no. 4, pp. 313-318, Apr. 1962.

[4] J. Nunzi, "Organic photovoltaic materials and devices," *Comptes Rendus Physique*, vol. 3, no. 4, pp. 523-542, May 2002.

[5] M. Green, "Silicon solar cells: Evolution, high-efficiency design and efficiency enhancements," *Semiconductor Science and Technology*, vol. 8, no. 1, pp. 1-12, Jan. 1993.

[6] European Commission, "PV Status Report 2009," Joint Research Centre; Renewable Energy Unit, 2009.

[7] M. Oliver and T. Jackson, "The market for solar photovoltaics," *Energy Policy*, vol. 27, no. 7, pp. 371-385, July 1999.

[8] J. Turner, "A realizable energy future," *Science*, vol. 285, no. 5428, pp. 687-689, July 1999.

[9] National Renewable Energy Laboratory (NREL), "Best Research Cell Efficiencies," 2011.

[10] V. Fthenakis and E. Alsema, "Photovoltaics energy payback times, greenhouse gas emission and external costs: 2004-early 2005 status," *Progress in Photovoltaics: Research and Applications*, vol. 14, no. 3, pp. 275-280, Mar. 2006.

[11] J. Szlufcik, S. Sivoththaman, J. Nlis, R. Mertens, and R. Van Overstraeten, "Low-cost industrial technologies of crystalline silicon solar cells," *Proceedings of the IEEE*, vol. 85, no. 5, pp. 711-730, May 1997.

[12] A. Muller, M. Ghosh, R. Sonnenschein, and P. Woditsch, "Silicon for photovoltaic applications," *Materials Science and Engineering: B*, vol. 134, no. 2, pp. 257-262, Oct. 2006.

[13] S. Forrest, "The path to ubiquitous and low-cost organic electronic appliances on plastic," *Nature*, vol. 428, no. 6986, pp. 911-918, Apr. 2004.

[14] F. Kessler and D. Rudmann, "Technological aspects of flexible CIGS solar cells and modules," *Solar Energy*, vol. 77, no. 6, pp. 685-695, May 2004.

[15] A. Morales-Acevedo, "Thin film CdS/CdTe solar cells: Research perspectives," *Solar Energy*, vol. 80, no. 6, pp. 675-681, June 2006.

[16] M. Gratzel, "Dye-Sensitized Solar Cells," *Journal of Photochemistry and Photobiology C*, vol. 4, no. 2, pp. 145-153, Oct. 2003.

[17] H. Hoppe and N. Sariciftci, "Organic solar cells: An Overview," *Journal of Materials Research*, vol. 19, no. 7, pp. 1924-1945, July 2004.

[18] G. Li, V. Shrotriya, J. Huang, Y. Yao, T. Moriarty, K. Emery and Y. Yang, "High-efficiency solution processable polymer photovoltaic cells by self-organization of polymer blends," *Nature Materials*, vol. 4, no. 11, pp. 864-868, Oct. 2005.

[19] M. Scharber, D. Muhlbacher, M. Koppe, P. Denk, C. Waldauf, A. Heeger, and C. Brabec, "Design rules for donors in bulk-heterojunction solar cells - towards 10% energy-conversion efficiency," *Advanced Materials*, vol. 18, no. 6, pp. 789-794, Feb. 2006.

[20] D. Chirvase, J. Parisi, J. Hummelen, and V. Dyakonov, "Influence of nanomorphology on the photovoltaic action of polymer-fullerene composites," *Nanotechnology*, vol. 15, no. 9, pp. 1317-1323, Sep. 2004.

[21] S. Shaheen, C. Brabec, and N. Sariciftci, "2.5% efficient organic plastic solar cells," *Applied Physics Letters*, vol. 78, no. 6, pp. 841-843, Feb. 2001.

[22] Y. Liang, Z. Xu, J. Xia, S. Tsai, Y. Wu, G. Li, C. Ray, and L. Yu, "For the bright future-bulk heterojunction polymer solar cells with power conversion efficiency of 7.4%," *Advanced Energy Materials*, vol. 22, no. 20, pp. E135-E138, May 2010.

[23] G. Yu, J. Gao, J. Hummelen, F. Wudl, and A. Heeger, "Polymer photovoltaic cells: Enhanced efficiencies via a network of internal donor-acceptor heterojunctions," *Science*, vol. 270, no. 5243, pp. 1789-1791, Dec. 1995.

[24] J. Kim, K. Lee, N. Coates, D. Moss, T. Nguyen, and A. Heeger, "Efficient tandem polymer solar cells fabricated by all-solution processing," *Science*, vol. 317, no. 5835, pp. 222-225, July 2007.

[25] K. Kawano, R. Pacios, D. Poplavskyy, J. Nelson, D. Bradley, and J. Durrant, "Degradation of organic solar cells due to air exposure," *Solar Energy Materials and Solar Cells*, vol. 90, no. 20, pp. 3520-3530, Dec. 2006.

[26] F. Krebs and H. Spanggaard, "Significant improvement of polymer solar cell stability," *Chemistry of Materials*, vol. 17, no. 21, pp. 5235-5237, Sep. 2005.

[27] S. Gunes, H. Neugebauer, and N. Sariciftci, "Conjugated polymer-based organic solar cells," *Chemical Reviews*, vol. 107, no. 4, pp. 1324-1338, Apr. 2007.

[28] F. Padinger, R. Rittberger, and N. Sariciftci, "Effect of postproduction treatment on plastic solar cells," *Advanced Functional Materials*, vol. 13, no. 1, pp. 85-88, Jan. 2003.

[29] H. Hoppe and N. Sariciftei, "Morphology of polymer/fullerene bulk heterojunction solar cells," *Journal of Materials Chemistry*, vol. 16, no. 1, pp. 45-61, Jan. 2006.

[30] W. Ma, C. Yang, X. Gong, K. Lee, and A. Heeger, "Thermally stable, efficient polymer solar cells with nanoscale control of the interpenetrating network morphology," *Advanced Functional Materials*, vol. 15, no. 10, pp. 1617-1622, Sep. 2005.

[31] J. Kim, S. Kim, H. Lee, K. Lee, W. Ma, X. Gong, and A. Heeger, "New architecture for high-efficiency polymer photovoltaic cells using solution-based titanium oxide as an optical spacer," *Advanced Materials*, vol. 18, no. 5, pp. 572-576, Mar. 2006.

[32] G. Li, V. Shrotriya, Y Yao, and Y. Yang, "Investigation of annealing effects and film thickness dependence of polymer solar cells based on poly(3-hexylthiophene)," *Journal of Applied Physics*, vol. 98, no. 4, p. 043704, Aug. 2005.

[33] P. King, T. Veal, F. Fuchs, C. Wang, D. Payne, A. Bourlange, H. Zhang, G. Bell, V. Cimalla, O. Ambacher, R. Egdell, F. Bechstedt, and C. McConville, "Band gap, electronic structure, and surface electron accumulation of cubic and rhombohedral In_2O_3," *Physical Review B*, vol. 79, no. 20, p. 205211, May 2009.

[34] A. Reed, L. Curtiss, and F. Weinhold, "Intermolecular interactions from a natural bond orbital, donor-acceptor viewpoint," *Chemical Reviews*, vol. 88, no. 6, pp. 899-926, Sep. 1988.

[35] G. Yu and A. Heeger, "Charge Separation and Photovoltaic Conversion in Polymer Composites with Internal Donor/Acceptor Heterojunctions," *Journal of Applied Physics*, vol. 78, no. 7, pp. 4510-4515, Oct. 1995.

[36] K. Coakley and M. McGehee, "Conjugated polymer photovoltaic cells," *Chemistry of Materials*, vol. 16, no. 23, pp. 4533-4542, Aug. 2004.

[37] R. Radbeh, E. Parbaile, J. Boucle, C. Bin, A. Moliton, V. Coudert, F. Rossignol, and B. Ratier, "Nanoscale control of the network morphology of high efficiency polymer fullerene solar cells by the use of high material concentration in the liquid phase," *Nanotechnology*, vol. 21, no. 3, p. 035201, Jan. 2010.

[38] Z. Bao, A. Dodabalapur, and A. Lovinger, "Soluble and processable regioregular poly(3-hexylthiophene) for thin film field-effect transistor applications with high mobility," *Applied Physics Letters*, vol. 69, no. 26, pp. 4108-4110, Oct. 1996.

[39] V. Mihailetchi, H. Xie, B. Boer, L. Koster, and P. Blom, "Charge transport and photocurrent generation in poly(3-hexylthiophene):methanofullerene bulk-heterojunction solar cells," *Advanced Functional Materials*, vol. 16, no. 5, pp. 699-708, Feb. 2006.

[40] H. Sirringhaus, P. Brown, R. Friend, M. Nielsen, K. Bechgaard, B. Langeveld-Voss, A. Spierling, R. Janssen, E. Meijer, P. Herwig, and D. Leeuw, "Two-dimensional charge transport in self-organized, high-mobility conjugated polymers," *Nature*, vol. 40, no. 6754, pp. 685-688, Aug. 1999.

[41] P. Vanlaeke, A. Swinnen, I. Haeldermans, G. Vanhoyland, T. Aernouts, D. Cheyns, C. Deibel, J. D'Haen, P. Heremans, J. Poortmans, and J. Manca, "P3HT/PCBM bulk heterojunction solar cells: relation between morphology and electro-optical characteristics," *Solar Energy Materials and Solar Cells*, vol. 90, no. 14, pp. 2150-2158, Sep. 2006.

[42] Y. Kim, S. Cook, S. Tuladhar, S. Choulis, J. Nelson, J. Durrant, D. Bradley, M. Giles, I. McCulloch, C. Ha, and M. Ree, "A strong regioregularity effect in self-organizing conjugated polymer films and high-efficiency polythiophene:fullerene solar cells," *Nature Materials*, vol. 5, no. 3, pp. 197-203, Mar. 2006.

[43] H. Ajie, M. Alvarez, S. Anz, R. Beck, F. Diederich, K. Fostiropoulos, D. Huffman, W. Kratschmer, Y. Rubin, K. Schriver, D. Sensharma, and R. Whetten, "Characterization of the soluble all-carbon molecules C_{60} and C_{70}," *Journal of Physical Chemistry*, vol. 94, no. 24, pp. 8630-8633, Nov. 1990.

[44] L. Echegoyen and L. Echegoyen, "Electrochemistry of fullerenes and their derivatives," *Accounts of Chemical Research*, vol. 31, no. 9, pp. 593-601, June 1998.

[45] R. Koeppe and N. Sariciftci, "Photoinduced charge and energy transfer involving fullerene derivatives," *Photochemical and Photobiological Sciences*, vol. 5, no. 12, pp. 1122-1131, Oct. 2006.

[46] L. Groenendaal, F. Jonas, D. Freitag, H. Pielartzik, and J. Reynolds, "Poly(3,4-ethylenedioxythiophene) and its derivatives: Past, present, and future," *Advanced Materials*, vol. 12, no. 7, pp. 481-494, Apr. 2000.

[47] D. Wohrle and D. Meissner, "Organic Solar Cells," *Advanced Materials*, vol. 3, no. 3, pp. 129-138, Mar. 1991.

[48] V. Lemaur, M. Steel, D. Beljonne, J, Bredas, and J. Cornil, "Photoinduced charge generation and recombination dynamics in model donor/acceptor pairs for organic solar cell applications: A full quantum-chemical treatment," *Journal of the American Chemical Society*, vol. 127, no. 16, pp. 6077-6086, Apr. 2005.

[49] L. Dalton, J. Thomson, and H. Nalwa, "The role of extensively delocalized π-electrons in electrical conductivity, non-linear optical properties and physical properties of polymers," *Polymer*, vol. 28, no. 4, pp. 543-552, Mar. 1987.

[50] I. Montanari, A. Nogueira, J. Nelson, J. Durrant, C. Winder, M. Loi, N. Sariciftci, and C. Brabec, "Transient optical studies of charge recombination dynamics in a polymer/fullerene composite at room temperature," *Applied Physics Letters*, vol. 81, no. 16, pp. 3001-3003, Aug. 2002.

[51] R. Marsh, J. Hodgkiss, S. Albert-Seifried, and R. Friend, "Effect of annealing on P3HT:PCBM charge transfer and nanoscale morphology probed by ultrafast spectroscopy," *Nano Letters*, vol. 10, no. 3, pp. 923-930, Feb. 2010.

[52] M. Compoy-Quiles, T. Ferenczi, T. Agostinelli, P. Etchegoin, Y. Kim, T. Anthopoulos, P. Stavrinou, D. Bradley, and J. Nelson, "Morphology evolution via self-organization and lateral and vertical diffusion in polymer:fullerene solar cell blends," *Nature Materials*, vol. 7, no. 2, pp. 158-164, Jan. 2008.

[53] L. Koster, V. Mihailetchi, and P. Blom, "Biomolecular recombination in polymer/fullerene bulk heterojunction solar cells," *Applied Physics Letters*, vol. 88, no. 5, p. 052104, Jan. 2006.

[54] M. Reyes-Reyes, K. Kim, and D. Carroll, "High-efficiency photovoltaic devices based on annealed poly(3-hexylthiophene) and 1-(3-methoxycarbonyl)-propyl-1-phenyl-(6,6)C_{61} blends," *Applied Physics Letters*, vol. 87, no. 8, p. 083506, Aug. 2005.

[55] Y. Kim, S. Choulis, J. Nelson, D. Bradley, S. Cook, and J. Durrant, "Device annealing effect in organic solar cells with blends of regioregular poly(3-hexylthiophene) and soluble fullerene," *Applied Physics Letters*, vol. 86, no. 6, p. 063502, Feb. 2005.

[56] J. Huang, P. Miller, J. Mello, A. Mello, and D. Bradley, "Influence of thermal treatment on the conductivity and morphology of PEDOT/PSS Films," *Synthetic Metals*, vol. 139, no. 3, pp. 569-572, Oct. 2003.

[57] M. Kim, B. Kim, and J. Kim, "Effective variables to control the fill factor of organic photovoltaic cells," *Applied Materials and Interfaces*, vol. 1, no. 6, pp. 1264-1269, May 2009.

[58] J. Woollam and P. Snyder, "Fundamentals and applications of variable angle specroscopic ellipsometry," *Materials Science and Engineering B*, vol. 5, no. 2, pp. 279-283, Jan. 1990.

[59] P. McMarr and K. Vedam, "Spectroscopic ellipsometry: A new tool for nondestructive depth profiling and characterization of interfaces," *Journal of Applied Physics*, vol. 59, no. 3, pp. 694-701, Feb. 1986.

[60] F. Celii, T. Harton, and O. Phillips, "Characterization of organic thin films for OLEDs using spectroscopic ellipsometry," *Journal of Electronic Materials*, vol. 26, no. 4, pp. 366-371, Apr. 1997.

[61] C. Brabec, A. Cravino, D. Meissner, N. Sariciftci, T. Fromherz, M. Rispens, L. Sanchez, and J. Hummelen, "Origin of the open circuit voltage of plastic solar cells," *Advanced Functional Materials*, vol. 11, no. 5, pp. 374-380, Oct. 2001.

[62] W. Wang, H. Wu, C. Yang, C. Luo, Y. Zhang, J. Chen, and Y. Cao, "High-efficiency polymer photovoltaic devices from regioregular-poly(3-hexylthiophene-2,5-diyl) and [6,6]-phenyl-C_{61}-butyric acid methyl ester processed with oleic acid surfactant," *Applied Physics Letters*, vol. 90, no. 18, p. 183512, May 2007.

[63] W. Baek, H. Yang, T. Yoon, C. Kang, H. Lee, and Y. Kim, "Effect of P3HT:PCBM concentration in solvent on performances of organic solar cells," *Solar Energy Materials and Solar Cells*, vol. 93, no. 8, pp. 1263-1267, Aug. 2009.

[64] S. Yoo, W. Potscavage, B. Domercq, S. Han, T. Li, S. Jones, R. Szoszkiewicz, D. Levi, E. Riedo, S. Marder, and B. Kippelen, "Analysis of improved photovoltaic properties of pentacene/C_{60} organic solar cells: effects of exciton blocking layer thickness and thermal annealing," *Solid-State Electronics*, vol. 51, no. 10, pp. 1367-1375, Oct. 2007.

[65] S. Miller, G. Fanchini, Y. Lin, C. Li, C. Chen, W. Su, and M. Chhowalla, "Investigation of nanoscale morphological changes in organic photovoltaics during solvent vapor annealing," *Journal of Materials Chemistry*, vol. 18, no. 3, pp. 306-312, Jan. 2008.

[66] American Society of Testing and Materials (ASTM), G-173-03, "Reference solar spectral irradiance," 2003.

[67] R. Friend, R. Gymer, A. Holmes, J. Burroughes, R. Marks, C. Taliani, D. Bradley, D. Dos Santos, J. Bredas, M. Logdlund, and W. Salaneck, "Electroluminescence in conjugated polymers," *Nature*, vol. 397, no. 6715, pp. 121-128, Jan. 1999.

[68] V. Shrotriya, J. Ouyang, R. Tseng, G. Li, Y. Yang, "Absorption spectra modification in poly(3-hexylthiophene):methanofullerene blend thin films," *Chemical Physics Letters*, vol. 411, no. 1, pp. 138-143, Aug. 2005.

[69] Y. Lan, "P3HT:PCBM bulk heterojunction solar cells characterization by spectroscopic ellipsometry," Horiba Scientific application note, 2011.

[70] G. Dennler, K. Forberich, M. Scharber, and C. Brabec, "Angle dependence of external and internal quantum efficiencies in bulk-heterojunction organic solar cells," *Journal of Applied Physics*, vol. 102, no. 5, pp. 054516, Sep. 2007.

[71] A. Ng, C. Li, M. Fung, A. Djurisic, J. Zapien, W. Chan, K. Cheung, and W. Wong, "Accurate determination of the index of refraction of polymer blend films by spectroscopic ellipsometry," *Journal of Physical Chemistry C*, vol. 114, no. 35, pp. 15094-15101, Aug. 2010.

[72] U. Zhokhavets, T. Erb, G. Gobsch, M. Al-Ibrahim, and O. Ambacher, "Relation between absorption and crystallinity of poly(3-hexylthiophene)/fullerene films for plastic solar cells," *Chemical Physical Letters*, vol. 418, no. 4, pp. 347-350, Feb. 2006.

[73] J. Jo, S. Na, S. Kim, T. Lee, Y. Chung, S. Kang, D. Vak, and D. Kim, "Three-dimensional bulk heterojunction morphology for achieving high internal quantum efficiency in polymer solar cells," *Advanced Functional Materials*, vol. 19, no. 15, pp. 2398-2406, July 2009.

[74] C. Liang, W. Su, and L. Wang, "Enhancing the Photocurrent in Poly(3-hexylthiophene/[6,6]-phenyl C_{61} Butyric Acid Methyl Ester Bulk Heterojunction Solar Cells by Using Poly(3-hexylthiophene) as a Buffer Layer," *Applied Physics Letters*, vol. 95, no. 13, p. 133303, Oct. 2009.

[75] M. Irwin, D. Buchholz, A. Hains, R. Chang, and T. Marks, "p-Type semiconducting nickel oxide as an efficiency-enhancing anode interfacial layer in polymer bulk-heterojunction solar cells," *Proceedings of the National Academy of Sciences of the United States of America*", vol. 105, no. 8, pp. 2783-2787, Feb. 2008.

[76] V. Shrotriya, G. Li, Y. Yao, C. Chu, and Y. Yang, "Transition metal oxides as the buffer layer for polymer photovoltaic cells," *Applied Physics Letters*, vol. 88, no. 7, p. 073508, Feb. 2006.

[77] M. Morana, M. Wegscheider, A. Bonanni, N. Kopidakis, S. Shaheen, M. Scharber, Z. Zhu, D. Waller, R. Gaudiana, and C. Brabec, "Bipolar charge transport in PCPDTBT-PCBM bulk-heterojunctions for photovoltaic applications," *Advanced Functional Materials*, vol. 18, no. 12, pp. 1757-1766, June 2008.

[78] M. Tong, N. Coates, D. Moses, and A. Heeger, "Charge carrier photogeneration and decay dynamics in the poly(2,7-carbazole) copolymer PCDTBT and in bulk heterojunction composites with $PC_{70}BM$," *Physical Review B*, vol. 81, no. 12, p. 125210, Mar. 2010.

[79] J. Peet, J. Kim, N. Coates, W. Ma, D. Moses, A. Heeger, and G. Bazan, "Efficiency enhancement in low-bandgap polymer solar cells by processing with alkane dithiols," *Nature Materials*, vol. 6, no. 7, pp. 497-500, May 2007.

VITA

KEVIN ANTHONY LATIMER

Department of Electrical and Computer Engineering
231 Kaufman Hall
Old Dominion University
Norfolk, VA 23529
Tel: (757) 683 3741

16 Redbud Lane
Newport News, VA 23602
Tel: (757) 810 7753
Email: klati002@gmail.com

Education

Master of Science, Electrical Engineering, Old Dominion University, 2011

Bachelor of Science, Electrical Engineering, Old Dominion University, 2010

Employment

Old Dominion Research Foundation, *Graduate Research Assistant*, 2010-2011